This Project has received funding from European Commission by means of Horizon 2020,
the EU Framework Programme for Research and Innovation, under Grant Agreement no.727348

Grant Agreement No. 727348

Project Acronym:

SOCRATCES

Project title:

SOlar Calcium-looping integRAtion for Thermo-Chemical Energy Storage.

DELIVERABLE D2.2

(Carbonator Model)

Funding scheme:	Research and Innovation Action (RIA)		
Project Coordinator:	USE		
Start date of the project:	01.01.2018	**Duration of the project:**	36 months
Contractual delivery date:	Month 12		
Actual delivery date:	23.12.2018		
Contributing WP:	WP2		
Dissemination level:	*Public*		
Authors:	Evgenios Karasavvas (CERTH), Nikos Vlachos (CERTH), Kyriakos Panopoulos (CERTH), George Karagiannakis (CERTH), Simira Papadopoulou (CERTH), Spyros Voutetakis (CERTH)		
Contributors:	Luis M Romeo (ZAR), Manuel Bailera (ZAR), Pilar Lisbona (ZAR), Luis I Diez (ZAR)		
Version:	V1		
Document name	**SOCRATCES_D2.2_v1**		

Table of contents:

INTRODUCTION

This deliverable refers to the work that is being carried out within Work Package 2 titled "Carbonation". The main objectives of the carbonation WP are to make an in-depth assessment of the carbonation reaction, develop a carbonator reactor at lab-scale, implement experiments for the understanding of the carbonation reaction and the its kinetics, all of which will subsequently provide useful data for the carbonator model development and the construction of the prototype reactor in the WP6. The carbonator reactor will also serve as a heat exchanger, as it will include a novel heat recovery system that comprises of cascading external tubes in which a heat transfer fluid will flow absorbing the produced carbonation heat, delivering it to the power block (D.4.1). In order to achieve the best carbonator operation conditions, analysis is carried out at lab-scale conditions (TGA and small-scale fixed bed reactors, or -optional- DRX, XPS, SEM, TEM) and scaled up by means of mathematical modelling. The carbonator is simulated using MATLAB, CFD and EES and/or other energy/power computer programs.

This document analyses the carbonator reactor performance through the development of different kinds, and level of detail, mathematical models, such as models that integrate heat, mass and momentum balances with reaction kinetics models. For example, the final conversion of the sorbent and the temperature profile of the carbonator constitute some of the most crucial process variables that affect both the carbonator performance and the final decisions for the prototype construction. Specifically, the main scope of the carbonator mathematical model development is to understand the performance and the respond of the reactor under different operation conditions and kinetics regimes and simultaneously conform with different technical and physical constraints. Also, the mathematical models' development will serve as a tool for the validation of them in WP7 by fine-tuning model parameters, where prototype experiments in the carbonator will be performed. In this way also, carbonation kinetics will be tested, and kinetics parameters will be refined in the real prototype plant conditions. Also, as the carbonator reactor works in tandem with a helical heat exchanger around it, a preliminary model development of it, is necessary also for the understanding of heat transfer phenomena. The deliverable summarizes the work under execution of Task 2.2 "*Carbonator development*". This task is divided in the following activities or subtasks:

- ST 2.2.1. Fluidization and sonication experiments
- ST 2.2.2. Preliminary reactor design with heat integration
- ST 2.2.3. Mathematical reactor modelling
- ST 2.2.4. Reactor process modelling
- ST 2.2.5. **Write up of deliverable (D2.2: carbonator model)**

Results from subtasks ST2.2.2 and ST2.2.3 are included in this deliverable (ST2.2.5) aiming to support the subtask ST.2.2.4.

The deliverable (D.2.2) is structured in three well-differentiated model sections.

In the first section, a 1-D heterogeneous steady state drop-tube carbonator model is described and presented by partner CERTH. Specifically, this model handles solids and gas as two distinct phases (gas and solid phase), with each phase characterized by individual physical properties (i.e., gas and solid phase density, specific heat, molecular weight etc.). Consequently, the model is based on an Euler-Euler approach, which means a segregated manipulation of each phase with the conservation of mass, energy, and momentum being used to couple them. Thus, the two phases are handled as fluids, and the plug flow assumption has been considered for both. Each phase possesses a finite volume fraction in each reactor section and the sum of them consist the total volume of the reactor. Mass (continuity equations), energy (first law of thermodynamics) and momentum (equation of Newtons second law) balances are constituting Navier – Stokes equations, simplified in one dimension, and solved for both phases. Kinetics are acquired from deliverable D2.1 (Carbonation kinetics) and the first WP2 internal report, where two different

("slow" and "fast") carbonation kinetic regimes has been developed. In this stage of the model development, the helical coiled heat exchanger has not been integrated in the aforementioned model due to the lack of significant data. This kind of carbonator model can be used also with high accuracy in more dense solids systems in which pressure and velocities variation have an important impact in the reactor's performance [1]. The solution of the model calculates the profile of several crucial variables along the reactor, such as: reactants conversion profile, pressure, gas and solid phase temperature, velocity and density, volume fraction of each phase and different variables related to heat transfer from the inner to the outer side of the reactor.

In the second section, a more simplistic carbonator model has been developed by partner ZAR. In this model, a 1-D steady state drop-tube carbonator model has been implemented. The gas phase is treated as a fluid with a plug flow assumption, while solids are modeled as a dilute entrained flow. Velocities of gas and solids are assumed constant, with the latter to be calculated from the terminal velocity of a falling particle in a medium. Also, pressure, void fraction of gas, and gas and solid phase properties are assumed constant too. Conversion profile of the sorbent is calculated via the residence time of gas and solids in the reactor using the same kinetics as the kinetics described in D2.1. Furthermore, the ZAR model includes a heat transfer model both for the inner part of the reactor, as for the outer, and the helical coiled heat exchanger which are all of them integrated with the reactor and the kinetic model. The model calculates the conversion of sorbent, the temperature of the carbonator and the temperature of the heat transfer fluid along the reactor, as well as the heat transfer in the Stirling's heat exchanger.

The third section describes the preliminary development of a 2-D axisymmetric CFD-based model for the carbonator by CERTH, which will provide useful insights for the coupled dynamics of the entrained solids and reactor flow as well as a more accurate way to predict thermal coupling of the particles with the reactor environment. Currently, the CFD-based model development does not include implementation of reaction dynamics. Also, via the CFD-based carbonator model, the main assumption of the plug flow of each phase will be investigated. Eventually, the axisymmetric CFD-based model intends to be coupled simultaneously with the carbonation reaction source terms to be solved for different operating conditions and then be compared to the other models. In this way, the CFD study is intended as an auxiliary tool both for the proper carbonator design and for verification of the 1-D carbonator models by CERTH and ZAR.

The document presented here has been developed within the SOCRATCES project under the confidentiality rules of the project and consortium.

1. 1-D CARBONATOR REACTOR MODEL (CERTH)

NOMENCLATURE

A Reactor cross-section area, [m^2]

$Alpha$ Pre-exponential factor, [atm]

a_{gp} Specific surface are between gas and particles, [$m^2\ m^{-3}$]

a_{gw} Specific surface are between gas and wall, [$m^2\ m^{-3}$]

C_D Drag force coefficient between particles and gas, [-]

C_{DS} Standard drag coefficient between a single particle and gas, [-]

Cp Specific heat capacity, [kJ $kg^{-1}\ k^{-1}$]

D Reactor diameter, [m]

d_p Particles diameter, [m]

E_2 Carbonation activation energy, [kJ mol^{-1}]

$F_{CO2,O}$ Initial molecular flow of CO_2, [mol s^{-1}]

$F_{CaO,O}$ Initial molecular flow of CaO, [mol s^{-1}]

F Molecular flow rate, [mol s^{-1}]

F_D Drag force between gas and solid, [kg $m^2\ s^{-2}$]

F_{fg} Friction force between gas and wall, [kg $m^2\ s^{-2}$]

F_{fs} Friction factor between solids and wall, [kg $m^2\ s^{-2}$]

Fr Froude number, $U_g/(gd_p)^{1/2}$ [-]

g Gravitational acceleration (9.81), [m s^{-2}]

G Solids mass flux (based on cross-sectional area of reactor), [kg $m^2\ s^{-1}$]

h_{gp} Heat transfer coefficient between interface of gas and solid phase, [W $m^{-2}\ K^{-1}$]

h_{gw} Heat transfer coefficient between gas and wall, [W $m^{-2}\ K^{-1}$]

k Thermal conductivity, [W $m^{-1}\ K^{-1}$]

$\dot{m}$ Mass flow rate, [kg s^{-1}]

MW_g Molecular weight of gas phase (44), [kg $kmol^{-1}$]

MW_s Molecular weight of solid phase, [kg $kmol^{-1}$]

MW_{CaO} Molecular weight of CaO (56), [kg $kmol^{-1}$]

MW_{CaCO3} Molecular weight of $CaCO_3$ (100), [kg $kmol^{-1}$]

N_s Number of solid particles per unit of reactor volume, [m^{-3}]

Nu Nusselt number, [-]

P Total pressure of reactor (based on partial pressure of CO_2), [Pa = kg $m^{-1}\ s^{-2}$]

P_{eq} Equilibrium pressure in temperature T and pressure P, [Pa]

Pr Prandtl number, $\mathrm{Pr} = \frac{Cp_g \mu_g .10^3}{k_g}$, [-]

Q_{gs} Thermal energy per meter of reactor transferred from solids to gas, [kW m^{-1}]

Q_{gw} Thermal energy transferred per meter from gas phase to the reactor wall, [kW m^{-1}]

Q_{gw_tot} *Total* thermal energy transferred from gas phase to the reactor wall, [kW]

Q_{rxn} Thermal energy per meter of reactor produced due to carbonation reaction , [kW m^{-1}]

Q_{rxn_tot} *Total* thermal energy produced at the end due to carbonation reaction, [kW]

r, $r(T,P)$ Reaction rate in Temperature T and Pressure P, [s^{-1}]

R Ideal gas constant (R = 8.314), [m^3 Pa mol^{-1} K^{-1}], (R = 8314.47), [Pa m^3 $kmol^{-1}$ K^{-1}]

$\dot{R}$ Consumption/Production term, [kmol m^{-3} s^{-1}]

Re_p Particle Reynolds number, $Re_p = \frac{\rho_p d_p |V_g - V_s|}{\mu_g}$, [-]

Re_g Gas Reynolds number, $Re_g = \frac{\rho_g U_g D}{\mu_g}$, [-]

T Temperature, [K or °C]

t Time, [s]

U_g Superficial gas velocity, [m s^{-1}]

v Cross-sectionally averaged velocity, [m s^{-1}]

X_k Maximum conversion of CaO at the end of the reaction

X Cross-sectionally averaged conversion, [-]

z, L Length of reactor, [m]

GREEK LETTERS

α_2 Pre-exponential factor, [s^{-1}]

Γ_s Net production rate due to heterogeneous reaction, [kg m^{-3} s^{-1}]

ΔH_{rxn} Enthalpy of carbonation reaction, [kJ mol^{-1}]

ΔH_2^o Standard enthalpy change of the overall reaction, [kJ mol^{-1}]

ΔS_2^o standard entropy change of carbonation reaction, [kJ mol^{-1}]

ε_g Cross-sectionally averaged voidage, [-]

ε_s Cross-sectionally averaged solid hold-up, [-]

λ_g Gas-wall friction coefficient, [-]

λ_f Solid-particle friction coefficient, [-]

μ Viscosity, [Pa s]

ρ Cross-sectionally averaged density, [kg m^{-3}]

ρ_{CaO} Particle CaO density, [kg m^{-3}]

ρ_{CaCO3} Particle $CaCO_3$ density, [kg m^{-3}]

SUBSCRIPT

CO_2 Carbon dioxide

CaO Calcium oxide

$CaCO_3$	Calcium carbonate
g	gas phase (CO_2)
o	initial
p	particle
s	solid phase (CaO)
w	Wall

1.1. Carbonator downer reactor design

As shown in Figure 1, the carbonator is a drop tube reactor which is divided into two sections, of two meters length each, comprising a four meters long reactor. Gas (CO_2) and solids (CaO) reactants are entering from the top, and the mixture of unconverted CaO and CO_2, and the $CaCO_3$ product are discharged from the bottom. Specifically, CaO particles are stored in a storage vessel in the top of the reactor, while normally a furnace will surround the vessel to preheat solids. CO_2 gas and CaO particles will enter the reactor while mass flow rate of each component will be controlled via a dosing system that will be set and established between CaO storage vessel on the top and first section of carbonator (not shown in the figure). A comprehensive review of downer reactors and solids dosing systems have been previously well presented [2]. Each carbonator section will be encircled by a helical coiled heat exchanger to remove produced heat during the exothermic reaction. The heat transfer fluid of the helical heat exchanger could be either an open loop fresh air, or a recirculated CO_2 stream as described at deliverable D4.1 (Figure 17). Externally of the carbonator and the helical heat exchanger, two furnaces will enclose each reactor section to provide the appropriate initial heat to the reactor for the start-up process. Also, the furnaces will ensure the manipulation of reactor's wall temperature by controlling power input of each furnace, comprising a secondary cooling system in tandem with the coiled heat exchanger. In this way, is will be guaranteed that appropriate heat is delivered to the power block and the Stirling engine. Finally, solids will be collected in a downward vessel in the bottom of the reactor (Figure 1).

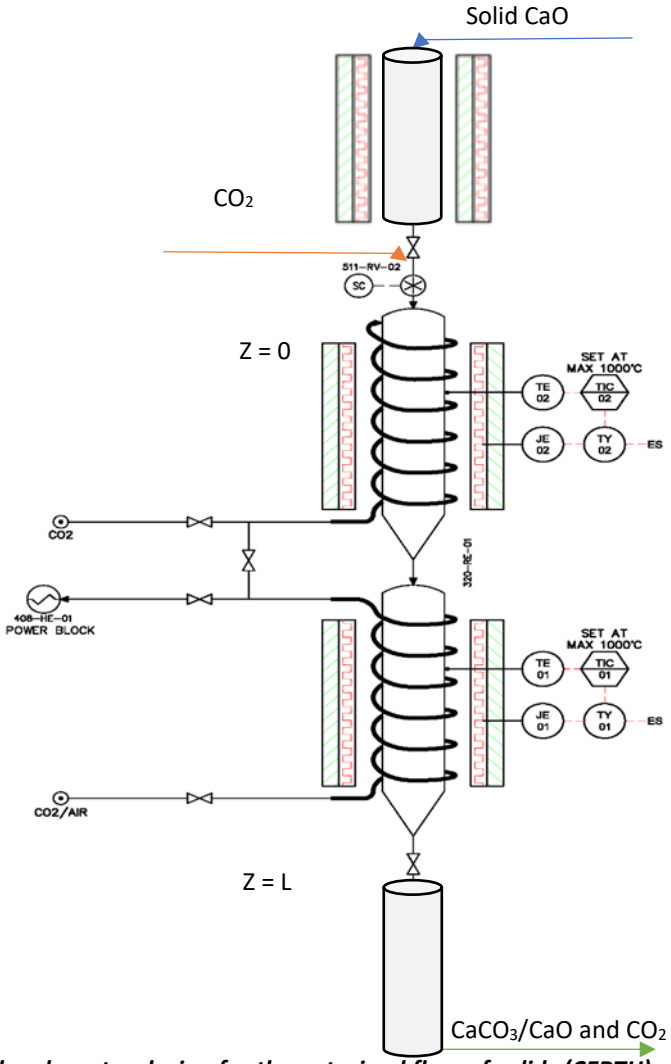

Figure 1. Conceptual carbonator design for the entrained flow of solids (CERTH)

1.2. Description of the drop-tube carbonator model

The major objective of the current field is the development of a detailed model of a drop tube, entrained flow carbonator reactor that will provide useful information about the reactor's performance and will be used later (WP7) for validation under prototype operation. Carbonator reactor must be functional in terms of high lime conversions at the end and efficient reaction heat exploitation must be achieved. For that reason, the first approach of the model will determine for the reactants (CaO and CO_2) conversions along the reactor length and temperature variation so. This is accomplished by the development of a 1-D reactor model that includes detailed mass and energy balances for the gas and the solid phase conjugated with momentum conservation. The system is modelled as it is comprised by two different phases, the gas (CO_2) and the solid (CaO & $CaCO_3$) phase. So, an Euler-Euler approach is used for both the gas and the solid phase, implying the continuity of each phase. Energy transfer to the cooling system of the reactor (coiled tubes) is not considered in this stage, but an assumption of a constant wall temperature and heat transfer through it is imposed. After the integration of a heat transfer model for both the reactor and the cooling system, the model will may eventually be used for dynamic studies and model-based dynamic optimization strategies.

Table 1 shows the methodology that have been followed for carbonator model development and the main assumptions of it.

Table 1. Methodology and assumptions of the carbonator model.

PARTNER	**CERTH**
EQUIPMENT	CARBONATOR
SOFTWARE	Matlab
SCOPE	Detailed simulations of carbonator reactor to assess performance and quantify heat transfer rates.
METHODOLOGY	
Chemical reactions kinetics: Deliverable 2.1 and 1st WP2 internal report.	
Fluid-dynamics: Continuity equations: Gas and solid phase balances (Euler-Euler approach), Momentum balance for gas and solid phase.	
Energy balances: Heat transfer: Heat transfer rated from solid to gas to wall, radiative heat transfer (to be implemented soon)	
ASSUMPTIONS	
• The downer reactor is modelled at steady state and at constant wall temperature conditions. • 1-D heterogeneous plug flow model for the gas and solid phase with respect to the reactor length. Discretization of 0.8 mm. • The radial dispersions of mass, momentum and energy are neglected. • The entrained-flow system is assumed to be very dilute in the solid phase such that the particle-wall and interparticle interactions may be neglected. Consequently, the conductive heat transfer between single particles and particles and wall is neglected. • The ideal gas law is assumed for the gas phase. • Solids assumed to be spherical, and uniform size and temperature inside them is considered. • The reaction kinetics are described by a Prout-Tompkins model (D2.1 or 1st WP2 internal report).	

- Kinetic energy and work forces of the system are negligible in comparison to the thermal energy due to high temperature in the carbonator.
- Gas phase physical properties (heat capacity, thermal conductivity and viscosity) are calculated from ASPEN PLUS properties (IDEAL).
- Solid phase heat capacity is assumed constant (ASPEN PLUS properties) while density varying between density of CaO and $CaCO_3$ as a function of conversion. Porous material

Table 2 illustrates initial input conditions of the model and model outputs. It is obvious that, except for initial flow rates, temperatures, and velocities values, that are easily defined, initial density of solid phase is quite unclear as it is an intrinsic material characteristic which varies from material to another and alters in an unspecified manner during the reaction. So, experimental measurements for final SOCRATCES material must be fulfilled to determine intrinsic properties such a bulk density and porosity variation through reaction. Thus, experimental work will provide insights to the model for more reliable results. Outputs of the model will provide useful information both for carbonation yield and the cooling strategy that must be implemented for the optimum heat exploitation.

Table 2. Inputs and outputs of carbonator simulation (CERTH)

PARTNER	**CERTH**
EQUIPMENT	CARBONATOR
SOFTWARE	Matlab
INPUT	**OUTPUT**
• Mass flow rate of CaO • Mass flow rate of CO_2 • Pressure • Voidage • Superficial velocity • Solid phase temperature • Gas temperature • Solid phase velocity • Gas phase velocity • Solid phase density • Gas phase density	• CaO and CO_2 conversion profile • Pressure variation along the reactor • Reaction rate variation along the reactor • Gas and solid phase temperature profile • Voidage variation along the reactor • Gas and solid phase velocity profile • Gas and solid phase density variation along reactor • Produced heat per meter due to reaction • Total produced heat due to reaction • Transferred heat per meter from solid to gas phase to wall • Total transferred heat from gas phase to wall

1.3. Carbonator model development

1.3.1. Continuity and hydrodynamic model

The hydrodynamic model is derived from the conservation of mass, energy and momentum to estimate the gas voidage, pressure and velocity variations of both phases along the axial direction of the downer carbonator at steady state conditions. In Tables below, (Tables 3,4), the differential form of continuity conservation, mass, energy and momentum balances for both phases (gas and solid phase) are illustrated among with supplementary algebraic equations for the hydrodynamics (Table 5)

Table 3. Mass, energy and momentum balance equations for solid phase.

Solid phase	
Continuity conservation $\frac{d((\varepsilon_s(\mathrm{z}))\rho_s(\mathrm{z})\,\mathrm{v}_s(\mathrm{z}))}{dz} = \dot{\Gamma}_{s-g}(\mathrm{z})(1-\varepsilon_g(\mathrm{z}))$	(1)
Momentum conservation $\frac{d(\varepsilon_s(\mathrm{z})\rho_s(\mathrm{z})\,\mathrm{v}_s{}^2(\mathrm{z}))}{dz} = F_D(z) - F_{fs}(z) + \varepsilon_s(z)\rho_s(z)g + F_{mass}(\mathrm{z})$	(2)
Species conservation $\frac{dX_{CaO}}{dz} = -\frac{A_s(\mathrm{z})}{F_{CaO,\mathrm{O}}}\dot{R}(\mathrm{z})$	(3)
Energy conservation $\frac{d(\mathrm{v}_s(\mathrm{z})\varepsilon_s(\mathrm{z})\rho_s(\mathrm{z})\,\mathrm{Cp}_s\mathrm{T}_s(\mathrm{z}))}{dz} = a_{gp}(\mathrm{z})h_{conv,gp}(\mathrm{z})(\mathrm{T}_g(\mathrm{z}) - \mathrm{T}_s(\mathrm{z})) + \Delta H_{rxn}\,\dot{R}(\mathrm{z})(1-\varepsilon_g(\mathrm{z}))$	(4)

In steady state conditions and ignoring the small non-uniformity in radial dimension [3], [4], the continuity equations for solid and gas phase in one dimension (z-dimension) are performed as shown in Tables 3,4 (Eqns.1,5). $\varepsilon_g, \rho_g, v_g$ is the voidage, density, and velocity of gas phase, and $\varepsilon_S, \rho_S, v_S$ the hold up, density and velocity of solid phase respectively. $\dot{\Gamma}_S$ and $\dot{\Gamma}_g$ denote the mass transfer rate per unit volume from one phase to another due to heterogeneous chemical reaction [5]–[11].

Table 4. Mass, energy and momentum balance equations for gas phase.

Gas phase	
Continuity conservation $\frac{d(\varepsilon_g(\mathrm{z})\rho_g(\mathrm{z})\,\mathrm{v}_g(\mathrm{z}))}{dz} = -\dot{\Gamma}_{s-g}(\mathrm{z})(1-\varepsilon_g(\mathrm{z}))$	(5)
Momentum conservation $\frac{d(\varepsilon_g(\mathrm{z})\rho_g(\mathrm{z})\,\mathrm{v}_g{}^2(\mathrm{z}))}{dz} = -\frac{dP}{dz} - F_D(z) - F_{fg}(z) + \varepsilon_g(z)\rho_g(z)g - F_{mass}(\mathrm{z})$	(6)
Species conservation $\frac{dX_{CO_2}}{dz} = \frac{F_{CaO,O}}{F_{CO_2,O}}\frac{dX_{CaO}}{dz}$	(7)
Energy conservation $\frac{d(\mathrm{v}_g(\mathrm{z})\varepsilon_g(\mathrm{z})\rho_g(\mathrm{z})\,\mathrm{Cp}_g(\mathrm{z})\,\mathrm{T}_g(\mathrm{z}))}{dz} = a_{gp}(\mathrm{z})h_{gp}(\mathrm{z})(\mathrm{T}_s(\mathrm{z}) - \mathrm{T}_g(\mathrm{z})) + a_{gw}(\mathrm{z})h_{gw}(\mathrm{z})(\mathrm{T}_w(\mathrm{z}) - \mathrm{T}_g(\mathrm{z}))$	(8)

The corresponding momentum conservation equations for gas and solid phase ignoring radial distribution of velocity and diffusion terms are presented in Tables 1,2 (Eqns.2,6) [1], [5]–[9], [12]–[16]. Also, in Table 5, the corresponding algebraic equations of momentum balances are illustrated [1], [5], [6], [9], [13], [14], regarding drag forces and coefficients among gas-solid phase and wall.

Equation 17 relates the volume fraction of solid and gas phase respectively [17].

Table 5. Equations related to hydrodynamics.

Drag force between solids and gas

$$F_D(z)=\frac{3}{4}\frac{C_D(z)}{d_p}(1-\varepsilon_g(z))(z)\rho_g(z)(\mathrm{v}_g(z)-\mathrm{v}_s(z)\,|\,\mathrm{v}_g(z)-\mathrm{v}_s(z)) \quad (9)$$

Drag coefficient

$$C_D(z)=\frac{14.1[1+2.78/(\mathrm{G}_g/\mathrm{G}_s)]}{Fr(z)}C_{DS}(z) \quad (10)$$

Standard drag coefficient

$$C_{DS}(z)=\begin{cases}\dfrac{24}{\mathrm{Re}_p(z)}(1+0.15\,\mathrm{Re}_p^{0.687}(z)), & \mathrm{Re}_p\le 1000\\ 0.44, & \mathrm{Re}_p>1000\end{cases} \quad (11)$$

Friction force between gas and wall

$$F_{fg}(z)=\frac{1}{2}\frac{\lambda_g(z)\rho_g(z)v_g^2(z)}{D} \quad (12)$$

Friction coefficient between gas and wall

$$\lambda_g(z)=\begin{cases}\dfrac{16}{\mathrm{Re}_g(z)}, & \mathrm{Re}_g\le 2300\\ \dfrac{0.079}{\mathrm{Re}_g^{0.313}(z)}, & \mathrm{Re}_g>2300\end{cases} \quad (13)$$

Friction force between particles and wall

$$F_{fs}(z)=\frac{1}{2}\frac{(\lambda_f(z)-\lambda_g(z))\rho_g(z)v_g^2(z)}{D} \quad (14)$$

Friction coefficient between particles and wall

$$\lambda_f=\frac{0.0285\sqrt{gD}}{(\mathrm{G}_s/\rho_s(z)\varepsilon_s(z))} \quad (15)$$

Momentum exchange between gas and solid phase due to chemical reaction [6], [9]

$$F_{mass}(z)=\dot{\Gamma}_{s-g}(z)v_g(z)(1-\varepsilon_g(z)) \quad (16)$$

Total volume conservation

$$\varepsilon_g(z)+\varepsilon_s(z)=1 \quad (17)$$

From the table above, (Table 5), F_D, is the drag force between gas and particles [1], [13], [18], while C_D is the drag coefficient which is obtained as a function of particles Reynolds number

[16], [17].C_{DS} is the standard drag coefficient and is a function of dimensionless Froude number [13], [18]. Moreover, F_{fg} and F_{fs} are the friction forces between gas-wall and gas-solids interface, while λ_f and $\lambda_g$the gas-wall and gas-solids friction coefficient [13].

The gas phase (CO_2) can be modelled as a compressible gas obeying the ideal gas low such that its density to be calculated from the following equation (Eqn.18). Also, from the ideal gas low, varying superficial gas velocity is calculated due to variation of pressure, gas phase temperature and gas phase molecular flow as shown below (Eqn.19). The model takes into consideration the modifications of particle characteristics as the carbonation reaction proceeds. The particle density ρ_s thus continuously varies between that of CaO particle density (ρ_{CaO}) and that of $CaCO_3$ (ρ_{CaCO3}) by a linear way as CaO conversion proceeds. In the same way, molecular weight of particles varies between that of CaO (MW_{CaO}) and $CaCO_3$ (MW_{CaCO3}) as shown in Table 5 (Eqn.21). G_g, and G_s are the total gas and solid mass flux based on cross-sectional area of the downer (A) and expressed by equations (22) and (23).

Table 6. Gas and solid phase density evolution, superficial gas velocity, solid phase molecular weight and gas and solid phase mass flux.

Gas phase density evolution
$$\frac{d\rho_g}{dz}+\frac{MW_g P(z)}{RT_g^2(z)}\frac{dT_g}{dz}-\frac{MW_g}{RT_g(z)}\frac{dP}{dz}=0 \quad (18)$$
Superficial velocity evolution
$$\frac{AP(z)}{F_{CO_2,O}R}\frac{dU_g}{dz}=-T_g(z)\frac{dX_{CO_2}}{dz}-\frac{(1-X_{CO_2}(z))T_g(z)}{P(z)}\frac{dP}{dz}+(1-X_{CO_2}(z))\frac{dT_g}{dz} \quad (19)$$
Solid phase density evolution
$$\frac{d\rho_s}{dz}+(\rho_{CaO}-\rho_{CaCO3})\frac{dX_{CaO}}{dz}=0 \quad (20)$$
Solid phase molecular weight evolution
$$MW_s(s)=X_{CaO}(s)MW_{CaCO_3}+(1-X_{CaO}(s))MW_{CaO} \quad (21)$$
Gas phase mass flux
$$G_g(z)=\varepsilon_g(z)\rho_g(z)v_g(z) \quad (22)$$
Solid phase mass flux
$$G_s(z)=(1-\varepsilon_g(z))\rho_s(z)v_s(z) \quad (23)$$

Where, *P*, is the pressure of gas phase, *R*, the ideal gas constant (8.314 Pa m^3 mol^{-1} K^{-1}), T_g, the temperature of gas phase, *A*, the average cross-section of the reactor, X_{CO2}, the conversion of CO_2 and $F_{CO2,0}$ the initial molecular flow rate of CO_2.

1.3.2.**Carbonation kinetics**

In this section the consumption/production terms of species are developed according to previous work that have been implemented, (Ortiz et al., 2018) and the contribution of AUTH and CISC (D2.1 and 1st WP2 internal report). The scope of this section is a model-approach calculation of the conversions of CaO and CO_2 along the reactor, which is developed under the following logic

The mass balance of a component (Plug Flow Reactor (PFR)) is given by the generic equation below:

$$\frac{\partial C}{dt} + \nabla(uC) = D\nabla^2 C + \dot{R}$$

In steady state conditions and ignoring the small non-uniformity of concentration in radial dimension and the diffusion terms, the mass balance of a component is reduced, and in a one-dimension (z-dimension) as follows:

$$\frac{\partial(\mathrm{uC})}{\partial z} = \dot{R} \rightarrow \frac{\partial F}{A\partial z} = \dot{R} \rightarrow \frac{\partial(F_O(1-\mathrm{X}))}{A\partial z} = \dot{R} \rightarrow \frac{dX}{dz} = -\frac{A}{F_O}\dot{R}$$

where A (m^2) is the cross-section of the phase (for one phase is the cross-sectional area of the reactor), F_O (mol s^{-1}) is the initial molecular flow of component and $\dot{R}$ (kmol m^{-3} s^{-1}) the production/consumption term.

Mathematical expression of $\dot{R}$ term

Several experiments have shown that the autocatalytic carbonation reaction is well fitted by a Prout-Tompkins model function $f(x) = X(1-X)$ modified by introducing a conversion limit, X_k, which is the CaO conversion at the end of the reaction-controlled phase [19]. Subsequently, the conversion rate of CaO have been presented by same authors, expressed as follows:

$$\frac{dX}{dt} = X\left(1-\frac{X}{X_k}\right)\mathrm{r}(\mathrm{T_s},\mathrm{P})$$

Thus, the expression used in the PFR model is shown in table (Table 7) below (Eqn.24), where X denotes the conversion of CaO and $r(T_s,P)$ a reaction rate expression in s^{-1} as a function of pressure P and temperature T_s (temperature of solid phase). ρ_S and MW_S is the particle density and molecular weight as reaction proceeds.

Table 7. Carbonation reaction kinetics.

<u>*Carbonation reaction rate*</u> $$\dot{R}(z) = \frac{dX_{CaO}}{dt}\frac{\rho_s(z)}{MW_s(z)} = X_{CaO}(\mathrm{z})\left(1-\frac{X_{CaO}(\mathrm{z})}{X_k}\right)\mathrm{r}(\mathrm{T},\mathrm{P})\frac{\rho_s(z)}{MW_s(z)} \quad (24)$$
<u>*Specific carbonation reaction rate*</u> [19] $$r \approx a_2 e^{\frac{-E_2}{RT_s}}\left(\frac{P}{P_{eq}}-1\right)\left(\frac{1}{\frac{P}{P_{eq}}+e^{\Delta S_2^o/R}e^{-\Delta H_2^o/RT_s}}\right) \quad (25)$$
<u>*Equilibrium pressure*</u> $$P_{eq} = Alpha\cdot e^{-a/\mathrm{T_s}}\cdot 101{,}325 \quad (26)$$

E_2 (kJ mol^{-1}) is the carbonation activation energy, a_2 (s^{-1}) is a pre-exponential factor, and R (kJ mol^{-1} K^{-1}) the gas constant. ΔH_2^o (kJ mol^{-1}) is the standard enthalpy change of the overall reaction, and ΔS_2^o (kJ mol^{-1} K^{-1}) the standard entropy change of carbonation. P_{eq} (atm) denotes the equilibrium pressure [19].

Alpha (atm) is a pre-exponential factor and a (K), an exponential factor for the reaction conditions of the same document. [19]

In Table 8, values of different parameters of Eq.26 are illustrated, while in Table 9 the re-fitted parameter a_2 of the Eq.25 is re-calculated in a range of 880-900 °C and 1.7 bar and the

respectively reaction rate *r* (in s^{-1}) is calculated. For this model a mean value of a_2 (74,666.66 s^{-1} and 42,255.33) is used and is assumed constant (with the expected discrepancies/deviations) in all simulation experiments that follows in the next sections.

Table 8. CO_2 Values of Enthalpy–Entropy changes in the chemical decomposition and desorption stages and activation energies [19]***.***

ΔH^0_r (kJ mol^{-1})	180
ΔH^0_1 (kJ mol^{-1})	160
ΔH^0_d (kJ mol^{-1})	20
E_d (kJ mol^{-1})	20
E_1 (kJ mol^{-1})	180
E_2(kJ mol^{-1})	20
ΔS^0_r (kJ mol^{-1} K^{-1})	0.16
ΔS^0_1 (kJ mol^{-1} K^{-1})	0.068
ΔS^0_d (kJ mol^{-1} K^{-1})	0.092
R (kJ mol^{-1} K^{-1})	0.008314
A (atm)	40,830,000
a (K)	20474

Experimental studies for the reaction rate of different particles (PSD 45-75 μm) of CaO in SOCRTACES conditions (1-1.7 bar, 800-900 °C) have been implemented by AUTH and CISC as described in Deliverable D2.1 and 1st WP2 internal report. From these studies, experimental values of CaO conversion versus time were perfectly fitted by Prout-Tompkins model re-adjusting a_2 parameter regarding to experiments. The values of experimentally fitted parameter a_2 that used in this model is illustrated in Table 9. Specifically, a mean value of parameter a_2 that emerged at a temperature range of 880-900 °C is used in the model development, and an assumption of constant a_2 value in a range of 600-900 is presumed. With this value specific carbonation reaction rate is calculated as carbonation proceeds.

Table 9. Calculated reaction rates and pre-exponential factors of carbonation reaction for the different studied temperatures (AUTH 1st WP2 internal report and D2.1).

T (°C)	880	890	900
Carbonation kinetics (1st WP2 internal report)			
r (s^{-1})	1.277	1.034	0.731
α2 (s^{-1}) (Eq. 26)	**45,826**	**43,171**	**37,769**
Carbonation kinetics (Deliverable D2.1)			
r (s^{-1})	2.07	1.80	1.46
α2 (s^{-1}) (Eq. 26)	**74,100**	**74,900**	**75,000**

1.3.3. **Energy balances**

In this work the energy balance of gas and solid phase is calculated. The scope of this section is the development of an adequate theoretical model approach which will calculate the distribution of gas and solid phase temperature along the reactor.

The energy balance of a component (Plug Flow Reactor (PFR)) has been given by the generic equation (kinetic energy of fluid and work forces are ignored) as presented at Tables 3,4 for gas and solid phase respectively.

Cp_g (kJ kg^{-1} K^{-1}) is the specific heat capacity of gas phase, T_g, T_s (K) the temperature of gas and solid phase respectively, and T_w (K) the reactor's wall temperature. a_{gp} (m^2 m^{-3}) and a_{gw} (m^2 m^{-3}) are defined as the specific surface area between gas and particles and gas and wall respectively.

In the table below, (Table 10), all the variables included at the energy balance of gas and solid phase are calculated:

Table 10. Variables calculation related to energy balances.

Specific surface between gas and particles [18]

$$a_{gp}(z) = \frac{6(1-\varepsilon_g(z))}{d_p} \quad (27)$$

Specific surface area between gas and wall [20]

$$a_{gw} = \frac{4}{D} \quad (28)$$

Heat transfer coefficient between gas and particles [21]

$$h_{gs}(z) = \frac{k_g Nu_{gs}(z)}{d_p} \quad (29)$$

Heat transfer coefficient between gas and wall [21]

$$h_{gw}(z) = \frac{k_g Nu_{gw}(z)}{D} \quad (30)$$

Gas-particles Nusselt number [21]

$$Nu_{gs}(z) = 2 + \sqrt{Nu^2_{gs,laminar}(z) + Nu^2_{gs,turbulent}(z)} \quad (31)$$

$$Nu_{gs,laminar}(z) = 0.644\left(\mathrm{Re}_p(z)\right)^{1/2}(\mathrm{Pr})^{1/3} \quad (32)$$

$$Nu_{gs,turbulent}(z) = \frac{0.0374\,\mathrm{Re}_s^{0.8}(z)\,\mathrm{Pr}}{1+2.443\,\mathrm{Re}_s^{-0.1}(z)(\mathrm{Pr}^{2/3}-1)} \quad (33)$$

Gas-wall Nusselt number (if Re_g<2300) [21]

$$Nu_{gw}(z) = (3.66^3 + 0.7^3 + (\mathrm{Nu}_1(z) - 0.7)^3 + \mathrm{Nu}_2^3(z))^{1/3} \quad (34)$$

$$Nu_1(z) = 1.615\left(\mathrm{Re}_g(z)\,\mathrm{Pr}\cdot\frac{D}{L}\right)^{1/3} \quad (35)$$

$$Nu_2(z) = 0.5\left(\frac{2}{1+22\,\mathrm{Pr}}\right)^{1/6}\left(\mathrm{Re}_g(z)\,\mathrm{Pr}\cdot\frac{D}{L}\right)^{1/2} \quad (36)$$

Gas-wall Nusselt number (if 2300<Re_g<10,000 [21]

$$Nu_{gw}(z) = (1-\gamma(z))\,\mathrm{Nu}_{\mathrm{lam},2300}(z) + \gamma Nu_{turb,10^4}(z) \quad (34.1)$$

$$\gamma(z) = \frac{\mathrm{Re}_g(z) - 2{,}300}{10^4 - 2{,}300} \quad (34.2)$$

$$\mathrm{Nu}_{\mathrm{lam},2300}(z) = \left\{49.371 + (\mathrm{Nu}_1(z) - 0.7)^3 + Nu_2{}^3(z)\right\}^{1/3} \quad (34.3)$$

$$\mathrm{Nu}_{\mathrm{turb},10^4}(z) = \frac{(0.0308/8)10^4\,\mathrm{Pr}(z)}{1+12.7\sqrt{0.0308/8}(\mathrm{Pr}^{2/3}(z)-1)}[1+\mathrm{D/L}]^{2/3} \quad (34.4)$$

$$\mathrm{Nu}_1(z) = 1.615(2300\,\mathrm{Pr(z)\,D/L}) \quad (35.1)$$

$$\mathrm{Nu}_2(z) = \left(\frac{2}{1+22\,\mathrm{Pr}(z)}\right)^{1/6}(2300\,\mathrm{Pr(z)\,D/L}) \quad (36.1)$$

$h_{conv,gp}$ (W m^{-2} K^{-1}) and $h_{conv,gw}$ (W m^{-2} K^{-1}) are the heat transfer coefficients between gas and particles interface and gas and wall respectively taking into consideration both laminar and turbulent transform mechanism.

k_g (W m^{-1} K^{-1}) is the thermal conductivity of gas phase and *Nu* the dimensionless Nusselt number.

The mathematical expressions used to calculate heat transfer coefficients have also been used by another study of the oxidation of copper in a downer reactor at high temperatures [20]. These correlations are used to calculate heat transfer coefficient between gas and wall and gas and particles. The correlations for gas-wall heat transfer coefficient (Eqns.34-36) are valid for different conditions. For example, the aforementioned correlations refer for all length of pipes, constant wall temperature, and can be derived for the mean Nusselt number during thermal and hydrodynamic development of laminar flow (Re_g<2300):

On the other hand, for heat transfer coefficient in the transition region between laminar and fully developed turbulent flow, similar correlations (Eqns.34.1-36.1) are used. After the critical Reynolds number (approximately 2300) is exceeded, the development of turbulence depends on many influencing factors, for example, the shape of the entrance of the tube, the manner in which the fluid flows towards the tube entrance and the disturbances in the velocity of the flow [21].

The aforementioned dimensionless numbers (gas and particle Reynolds number, Froude and Prandtl) are presented at the Table below (Table 11).

Table 11. Dimensionless numbers calculation.

Gas phase Reynolds number
$$\mathrm{Re}_g(z) = \frac{\rho_g(z) U_g(z) D}{\mu_g} \quad (37)$$
Solid phase Reynolds number
$$\mathrm{Re}_p(z) = \frac{\rho_g(z) d_p \lvert \mathrm{v}_g(z) - \mathrm{v}_s(z) \rvert}{\mu_g} \quad (38)$$
Froude number
$$Fr(z) = \frac{U_g(z)}{\sqrt{g d_p}} \quad (39)$$
Prandtl number
$$\mathrm{Pr} = \frac{Cp_g \cdot 10^3 \cdot \mu_g}{k_g} \quad (40)$$

In Table 12, some equations relative to transferred thermal energy are described. Specifically, the thermal energy, Q_{rxn} (kW m^{-1}), that produced due to carbonation reaction at solids surface per length of reactor is calculated by equation 41. This is an important index that indicates the rate of released energy in every part of reactor, giving significant insights for the cooling strategy of reactor. Also, from equation 42, the total produced thermal energy (Q_{rxn_tot}) due to reaction is calculated with the final sorbent conversion.

Moreover, the total thermal energy per length of reactor, Q_{gs}, (kW m^{-1}), that transferred from solids to gas is calculated from equation 43, where N_s is the number of solid particles per unit of reactor volume [16].

The total thermal energy that transferred from the gas phase to the reactor wall, Q_{gw_tot} (kW), is calculated from Eq.45. In this case, to calculate the total transferred energy, $h_{conv,gw}$, and ΔT, constitute the average convective heat transfer coefficient and the mean temperature difference between the gas phase and the wall, where δz, (m) denotes the step length of integration, $L/\delta z$, is the number of steps along the reactor. Among a step of integration δz, heat transfer coefficient and gas temperature are calculated by the mean value of the previous step i, and the next step $i+1$. The transferred thermal energy per length of the reactor Q_{qw} (kW m^{-1}) is calculated by the equation 46 and emanated by the division of equation 45 with δz.

Table 12. Transfer / thermal energy terms.

Produced thermal energy due to carbonation reaction per length of reactor
$$Q_{rxn}(z) = F_{CaO,0} \frac{dX_{CaO}}{dz} \Delta \mathrm{H}_{rxn} \quad (41)$$
Total energy produced at the end of carbonation reaction
$$Q_{rxn\_tot}(z) = F_{CaO,0}(1 - \mathrm{X}_{\mathrm{CaO}}) \Delta \mathrm{H}_{rxn} \quad (42)$$
Total energy transferred from solids to gas per length of reactor [16]
$$Q_{gs}(z) = A \cdot N_s(z) \cdot \pi \cdot d_p^2 \cdot h_{conv,gs}(z) \cdot (\mathrm{T}_s(z) - T_g(z)) \quad (43)$$

$$N_s(z) = \frac{6A(1-\varepsilon_g(z))}{A \cdot \pi \cdot d_p^3} \quad (44)$$

Total energy transferred from gas phase to the wall

$$Q_{gw\_tot}(z) = \pi \cdot D \cdot \delta z \cdot \sum_{i=1}^{L/\delta z} \left(\frac{h_{conv,gw,i+1} + h_{conv,gw,i}}{2} \right) \left(\frac{T_{g,i+1} + T_{g,i}}{2} - T_W \right) \quad (45)$$

Transferred thermal energy from gas phase to the wall per length of reactor

$$Q_{gw}(z) = \pi \cdot D \cdot \sum_{i=1}^{L/\delta z} \left(\frac{h_{conv,gw,i+1} + h_{conv,gw,i}}{2} \right) \left(\frac{T_{g,i+1} + h_{g,i}}{2} - T_W \right) \quad (46)$$

1.3.4. **Thermophysical properties**

All the thermophysical properties of CO_2 have been used from NIST data adopted from ASPEN PLUS software. Specifically, the calculation of specific heat capacity is adopted from NIST Aly-Lee 1981 ideal gas equation (CPIALEE) which is of the polynomial form as follows:

$$C_p^{*,ig} = C_{1i} + C_{2i}\left(\frac{C_{3i}/T}{\sinh(C_{3i}/T)}\right)^2 + C_{4i}\left(\frac{C_{5i}/T}{\cosh(C_{5i}/T)}\right)^2 \text{ for} C_{6i} \le T \le C_{7i}$$

CO_2 experimental and validated data from the aforementioned equation range from 50-4500 Kelvin. For SOCRATCES conditions NIST ASPEN PLUS data in the range of 270-1600 Kelvin have been fitted in a second order polynomial equation (R^2 = 0.9968) that emerged as illustrated below (Eqn.47).

Similarly, data also adopted for the viscosity of CO_2 in the range of 270-1600 Kelvin from NIST ThermoML Polynomial equation (MUVTMLPO) which is in the form of:

$$\eta_i^{*,v} = \sum_{m=1}^{nTerms} C_{mi} T^{m-1}$$

The equation arisen is a second order polynomial (R^2 = 0.9998) and is depicted below (Eqn.48).

Finally, the thermal conductivity is computed from NIST ThermoML Polynomial equation (KVTMLPO) in the range of 250-951 Kelvin.

$$\lambda_i^{*,v} = \sum_{m=1}^{nTerms} C_{mi} T^{m-1}$$

Here a liner regression model (R^2 =0.9997) was used to fit experimental data (Eqn.49).

Table 13. Thermophysical properties of CO_2.

Specific heat capacity of gas phase

$$Cp_g = -3 \cdot 10^{-7} T^2_{CO_2} + 9 \cdot 10^{-4} T_{CO_2} + 0.6316 \quad (47)$$

Dynamic viscosity of gas phase

$$\mu_g = -9 \cdot 10^{-12} T^2_{CO_2} + 5 \cdot 10^{-8} T_{CO_2} + 10^{-6} \quad (48)$$

Thermal conductivity of gas phase

$$k_g = 8 \cdot 10^{-5} T_{CO_2} - 0.007 \quad (49)$$

For temperatures greater than 951 K, a linear extrapolation is used.

2. MODEL ANALYSIS (CERTH)

The model of the downer carbonator consists of 38 algebraic equations (Eqns. (9)-(17), (21)-(49), and 11 differential equations (Eqns. (1)-(8), (18)-(20)), and the number of variables involved is 54, which can be classified into two groups: Design variables (N_{DV} = 5) and predicted variables (N_{PV} = 49). The 5 design variables must be predetermined in order the system to be well-posed. Also, the 17 process parameters integrate the mathematical model. The classification of parameters and variables are shown in Table 14.

Table 14. Classification of variables in the carbonator downer reactor.

Known Parameters/Variables	
Process parameters	g, d_p, MW_g, R, ρ_{CaO}, ρ_{CaCO3}, X_k, a_2, E_2, ΔS^0_2, ΔH^0_2, $Alpha$, a, C_{ps}, $\Delta H_{rxn,}$ MW_{CaO}, MW_{CaCO3}
Design variables	D, L, $F_{CO2,O}$, $F_{CaO,O}$, T_w
Predicted variables	
Differential variables	ε_g, P, U_g, T_s, X_{CaO}, X_{CO2}, T_g, ρ_s, ρ_g, v_s, v_g
Algebraic variables	ε_s, $\dot{\Gamma}_{gs}$, F_D, F_{fg}, F_{fs}, C_D, C_{DS}, Fr, G_s, G_g, Re_p, Re_g, λ_g, λ_f, $\dot{R}$, r, P_{eq}, a_{gp}, a_{gw}, h_{gp}, h_{gw}, Nu_{gs}, $Nu_{gs,laminar}$, $Nu_{gs,turbulent}$, Nu_{gw}, Nu_1, Nu_2, Pr, Q_{rxn}, Q_{gs}, N_s, Q_{gw_tot}, Q_{qw_tot}, Q_{gw} , Cp_g, μ_g, k_g, MW_s

Subsequently, the system constitutes of 49 equations (N_E) and 54 variables (N_V). Hence the degrees of freedom (N_F) are calculated as:

$$N_F = N_V - N_E = 54 - 49 = 5$$

3. MODEL SOLUTION (CERTH)

The problem is a DAEs (Differential and algebraic equations) system comprised by 11 first-order differential and 38 algebraic equations which are integrated simultaneously by a first-order backward finite difference method. In this work the mathematical model is coded in Matlab environment and numerically solved by a Matlab solver for stiff differential equations with a multistep solver option.

The developed system of DAEs can be treated an initial value problem. An initial value for each differential variable must be set for the integration initiation. Specifically, indicatives initial values for one operation scenario of the carbonator are depicted in Table 15.

Table 15. Initial values for an operation scenario of carbonator.

Gas voidage $\varepsilon_{g,0}$, [-]	0.95
Pressure P_0, [Pa]	100,000
Superficial velocity $U_{g,0}$, [m s^{-1}]	0.6037
CaO conversion $X_{CaO,0}$, [-]	0.005
CO_2 conversion $X_{CO2,0}$, [-]	0.000
Gas phase velocity $v_{g,0}$, [m s^{-1}]	0.6160
Solid phase velocity $v_{s,0}$, [m s^{-1}]	0.0055
Gas phase temperature $T_{g,0}$, [°C]	600

Solid phase temperature $T_{s,0}$ [°C]	600
Gas phase density $\rho_{g,0}$, [kg m^3]	1.0308
Solid phase density $\rho_{s,0}$, [kg m^3]	1600

In Table 16, the process parameters are illustrated and correspond to SOCRATCES conditions. The specific heat capacity of solid phase is assumed constant in a reasonable value. Also, the enthalpy of the carbonation reaction assumed constant with temperature.

Table 16. Selected model parameters.

Process parameters	Value
dp (m)	$75 \cdot 10^{-6}$
X_k *(-)*	0.691 or 0.150
ρCaO *(kg m^{-3})*	3,350
$\rho CaCO_3$ *(kg m^{-3})*	2,700
g (m s^{-2})	9.81
MW_g *(kg kmol^{-1})*	44.0
MW_{CaO} *(kg kmol^{-1})*	56.07
MW_{CaCO3} *(kg kmol^{-1})*	100.08
R (kJ mol^{-1} K^{-1} or m^3 mol^{-1} Pa^{-1} or Pa m^3 Kmol^{-1} K^{-1})	0.08314 or 8.314 or 8,314
a_2 *(s^{-1})*	74,666.66 or 42,255.33
E_2 *(kJ mol^{-1})*	20
ΔS^0_2 *(kJ mol^{-1}K^{-1})*	-0.068
ΔH^0_2 *(kJ mol^{-1})*	-160
Alpha (atm)	$4.083 \cdot 10^7$
a (K)	20,474
Cp_s *(kJ kg^{-1} K^{-1})*	1.00
ΔH_{rxn} *(kJ mol^{-1})*	178.7

On the other hand, although precise SOCRATCES conditions for carbonation reaction are not completely specified, it is considered reasonable to examine parametrically a range of operational conditions for the carbonator as shown in Table 17. Thus, a molecular flow ratio of 1:1 to 5:1 CO_2/CaO is examined through different input temperatures of reactants (600-800 °C). Also, the maximum conversion of CaO is consider high for the first cycle of the material (Xk = 0.691 [19]) and after the 10th cycle a residual maximum conversion value is set (D2.1 and 1st WP2 internal report) as Xk = 0.15. In this way, carbonator reactor is simulated both for the first cycle and for the actual conditions within SOCRATCES prototype continuous operation. Moreover, a parametric analysis of the mean particles diameter is employed to investigate the impact of if in the carbonator performance.

Table 17. Base case input data for simulation activities.

BASE CASE INPUT DATA
• Initial reactants temperature, T_{in}: 600-800 ^{O}C (Parametrically studied) • Initial pressure, P: 1.0 bar • Initial CaO flow rate, m_{CaO}: 12.74 kg h^{-1} • Initial CO_2 flow rate, m_{CO2}: 10-50 kg h^{-1} (Parametrically studied) • Reactor diameter, D: 0.1611 m • Reactor length, L: 4m • Solids diameter, d_p:5-170 μm (Parametrically studied) • Reactors wall temperature, T_w: 300-700 ^{o}C (Parametrically studied) • Maximum sorbent conversion, Xk: 15%, 69.1%

4. RESULTS AND DISCUSSION (CERTH)

4.1. Reactor performance under high maximum sorbent conversion and "slow" kinetics

4.1.1. Reactor's wall temperature and inlet reactants temperature analysis

A several number of simulations activities are presented in the next sections to investigate carbonator performance under different operation regimes with the kinetics as described in the 1st WP2 internal report. Specifically, as pointed out in a previous section (Model Analysis CERTH), five design variables (D, L, m_{CaO}, m_{CO2}, T_w) are emerged, which can fully define the system if reasonable values are set to them. Diameter of carbonator reactor, D, has been predetermined within Work Package 6 at 6" (D = 0.1611m) schedule 40 to ensure as low gas phase velocities as possible to ensure greater residence times for solids. Length of reactor, L, has also been predetermined at 4 meters (WP6) according to CERTH facilities height constraints. Mass flow rate of calcium oxide solids (CaO) has also fixed in a value of 12.74 kg h^{-1} according to the requirements for heat production and storage (D.4.1). Thus, mass flow rate of CO_2, m_{CO2}, and temperature of carbonator wall, T_w, constitute free variables to be parametrically studied. The value range of these variables are indicative and constitute reasonable values of the final prototype reactor operation (Table 17).

In this section, the effect of wall temperature, T_w (300 ^{o}C, 500 ^{o}C, 700 ^{o}C) and the reactants inlet temperature, T_{in} (600 ^{o}C, 700 ^{o}C, 800 ^{o}C) is initially examined respect to crucial reactor variables such as: Calcium oxide and CO_2 conversions (X_{CaO}, X_{CO2}), temperatures of gas and solid phase (T_g, T_s) (which represent carbonator temperature), produced heat due to reaction, transferred energy from solid to gas phase and transferred energy from gas phase to wall per length of reactor (Q_{rxn}, Q_{gp}, Q_{qw}) and finally velocity of gas and solid phase (v_g, v_p) (Figure 2). In this case, CO_2 mass flow rate (10 kg h^{-1}) has been chosen such as to correspond in stoichiometric molecular ratio (CO_2/CaO = 1/1). Maximum sorbent conversion is set at 69.1% corresponding to the first carbonation cycle of the solids [19], while particles diameter is set 75 μm as a reasonable value within SOCRATCES prototype plant operation.

Carbonation reaction has a very abrupt reaction rate in the first meter of the reactor as indicated by the very narrow curve of the rate of the produced energy due to reaction (Figure 2c) (~4.7 kW m^{-1}). Thus, that leads to a rapid approach of the equilibrium temperature (~890 ^{o}C) due to the highly exothermic reaction (Figure 2b). As soon as system reaches equilibrium temperature (Figure 2b), reaction rate diminishes to a residual constant value as shown by the constant rate of producing energy (Figure 2c). Therefore, by then, conversion rate of sorbent follows a constant linear trajectory up to the end of reactor (Figure 2a). The final sorbent conversion is

highly affected by wall temperature, as the lower the wall temperature, the faster the cooling rate of the reactor and so the greater the final conversion (~22-37%) (Figure 2a). The sharp increase of gas phase temperature (Figure 2b), follows a milder increase of gas and subsequently solid phase actual velocity (Figure 2d), while a gradual decrease of them is observed after system has reached equilibrium temperature and carbonation reaction proceeds linearly. It is observed that there is a constant divergence of solid phase velocity from gas phase (Figure 2d), which is justified due to gravitational forces, acceleration and buoyancy acting at solids (Eqn.2).

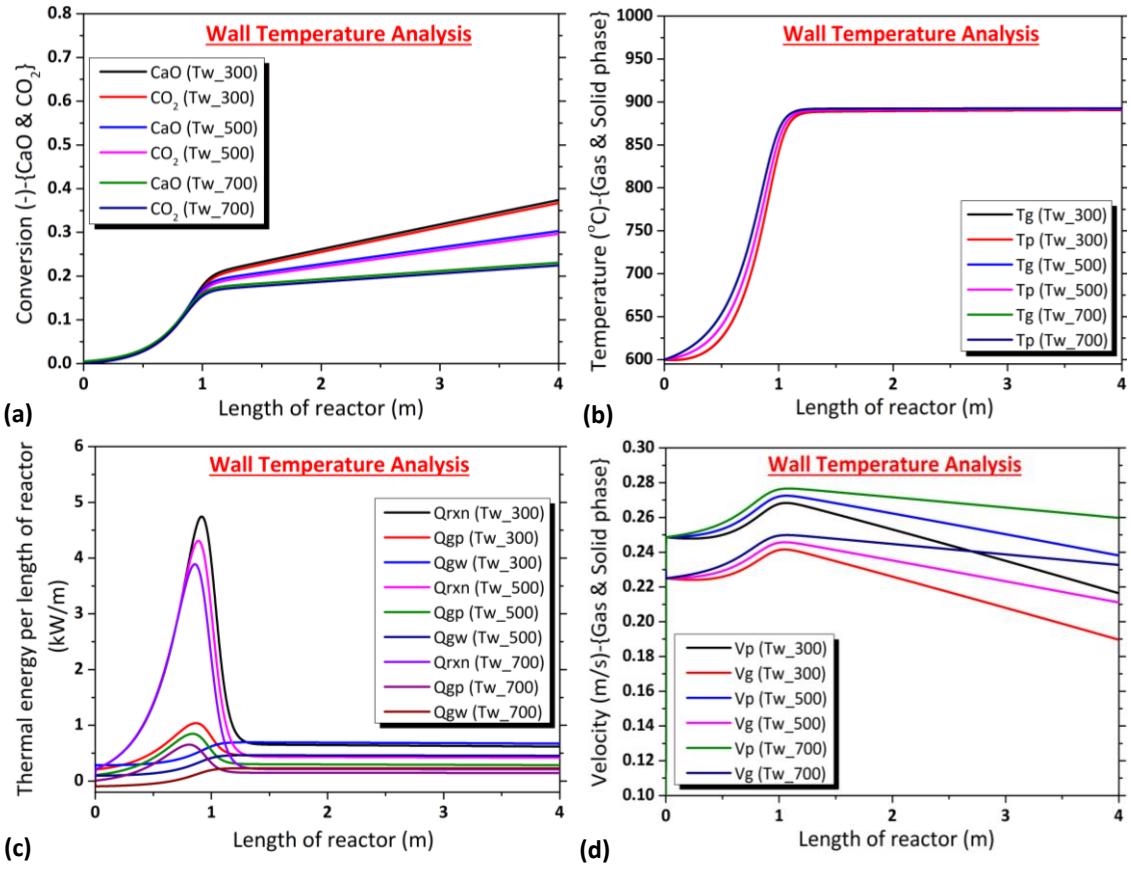

Figure 2. Comparison of the crucial process variables profiles under the three different reactor's wall temperatures (300, 500, 700 °C) and with constant initial reactants temperature, T_{in} = 600 °C; respect to the: (a) Conversion of CaO and CO_2, X_{CaO}, X_{CO2}; (b) Temperatures of gas and solid phase, T_g, T_s; (c) Thermal energy produced due to reaction, transferred from solid to gas phase and transferred from gas phase to wall per length of reactor, Q_{rxn}, Q_{gp}, Q_{qw}; (d) Velocity of gas and solid phase (v_g, v_p).

In correspondence with the previous one, the next graph, (Figure 3), illustrates the same carbonator variables, but with higher initial reactants temperature (T_{in} = 700 °C). Being reasonable, the evolution of all variables follows the same trend with the previous case. Reaction rate displays a pick within the first meter of the reactor, (Figure 3c) (~2.7 kW m^{-1}), leading very rapidly again to the equilibrium temperature (Figure 3b) (~890 °C). Compared with the previous case, sorbent conversions range in slightly lower values (Figure 3a) (~18-32%) due to higher wall temperature that imposes slower cooling rate of the reactor. The same trend with the previous case is observed also for the gas and solid phase velocities that range between 0.20-0.25 m s^{-1} and 0.23-0.28 m s^{-1} respectively (Figure 3d).

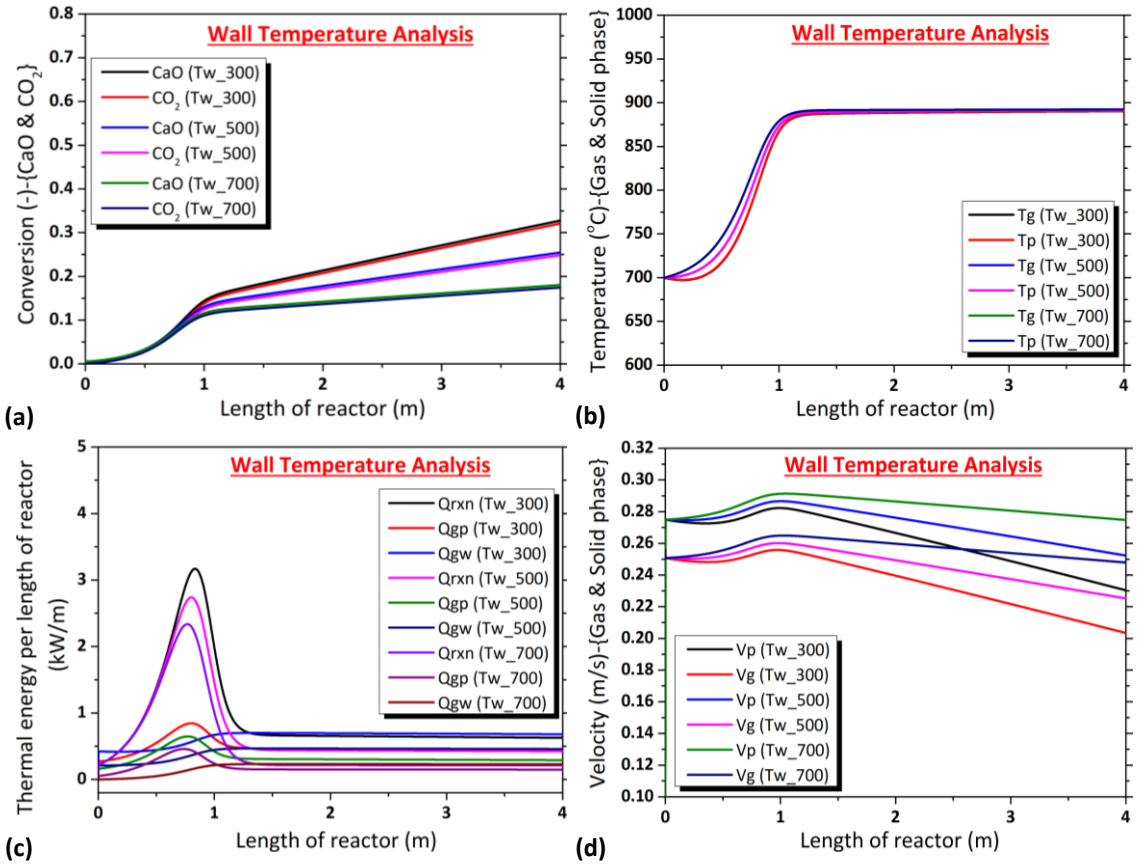

Figure 3. Comparison of the crucial process variables profiles under the three different reactor's wall temperatures (300, 500, 700 °C) and with constant initial reactants temperature, T_{in} = 700 °C; respect to the: (a) Conversion of CaO and CO_2, X_{CaO}, X_{CO2}; (b) Temperatures of gas and solid phase, T_g, T_s; (c) Thermal energy produced due to reaction, transferred from solid to gas phase and transferred from gas phase to wall per length of reactor, Q_{rxn}, Q_{gp}, Q_{qw}; (d) Velocity of gas and solid phase (v_g, v_p).

In correspondence with the previous cases, the next graph, (Figure 4), illustrates the same carbonator variables, but with the higher initial reactant's temperature (T_{in} = 800 °C). The evolution of all the variables follows the same trend with the previous cases. Reaction rate displays a pick within the first meter of the reactor, (Figure 4c) (~1.3 kW m^{-1}), leading very rapidly again to the equilibrium temperature (Figure 4b) (~890 °C). Compared with the previous cases, sorbent conversions range in the lowest values (Figure 4a) (~13-20%) due to higher wall temperature that imposes slower cooling rate of the reactor. The same trend with the previous cases is observed also for the gas and solid phase velocities that range between 0.22-0.26 m s^{-1} and 0.25-0.29 m s^{-1} respectively (Figure 4d).

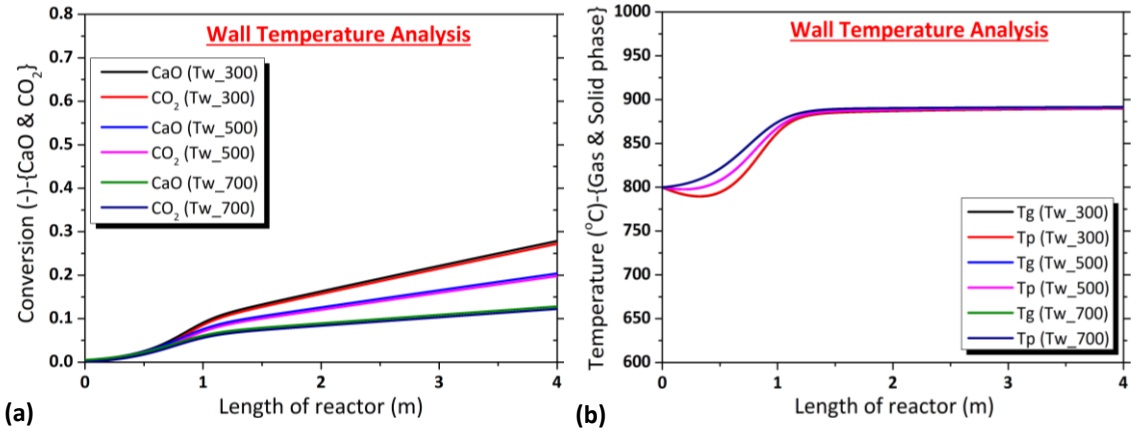

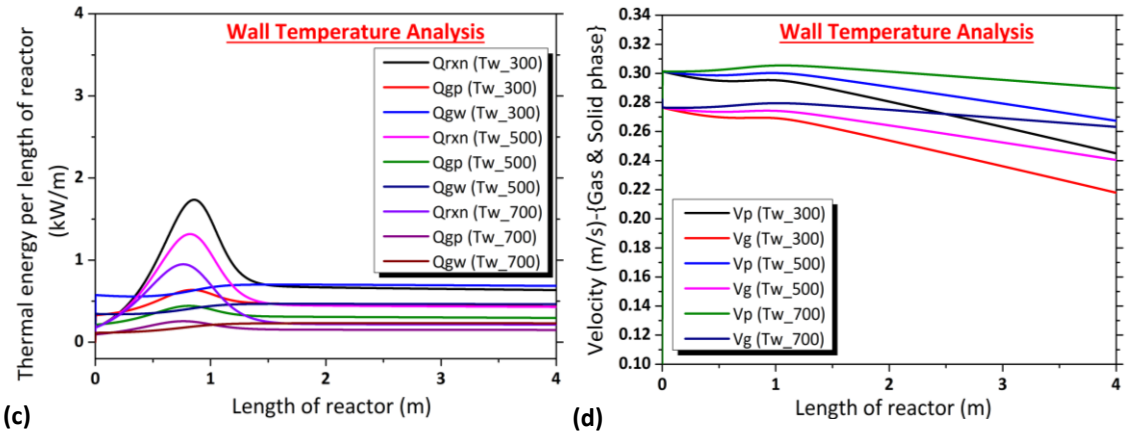

Figure 4. Comparison of the crucial process variables profiles under the three different reactor's wall temperatures (300, 500, 700 °C) and with initial reactants temperature, T_{in} = 800 °C; respect to the: (a) Conversion of CaO and CO_2, X_{CaO}, X_{CO2}; (b) Temperatures of gas and solid phase, T_g, T_s; (c) Thermal energy produced due to reaction, transferred from solid to gas phase and transferred from gas phase to wall per length of reactor, Q_{rxn}, Q_{gp}, Q_{qw}; (d) Velocity of gas and solid phase (v_g, v_p).

4.1.2. CO_2 excess analysis

In this section, the CO_2/CaO molecular ratio is parametrically studied subjected to the same process variables as previous. Specifically, CO_2/CaO molecular ratios from 2:1 to 5:1 are examined. From the previous section, it was chosen to fix initial reactant's temperature and wall temperature at 600 °C and 500 °C respectively. As for the initial reactant's temperature, 600 °C not only reflects to better results with respect to the sorbent conversion (Figure 2a, 3a, 4a), but also constitutes a more easily reached and technically feasible temperature for the prototype carbonator operation. Moreover, kinetic data of carbonation reaction are illustrated until the minimum temperature of 600 °C (D2.1 and 1st WP2 internal report) [19]. Lower temperatures will exceed kinetic model accuracy and is omitted in this stage of the model development. Wall temperature value is set constant at 500 °C representing a well-defined scenario neither underestimating nor overestimating it. Obviously, a more detailed energy model will be implemented afterwards which will integrate energy balances for both the wall of reactor and the helical heat exchanger but also will contain radiative heat transfer mechanisms. Furthermore, the same particles diameter (d_p = 75 μm) and maximum sorbent conversion are assumed (Xk = 0.691).

In the next graphs (Figures 5,6), the CO_2 excess subjected to different variables is examined. As the CO_2 excess increases, a severe inhibitory effect in the reaction rate initiation is observed (Figures 5c). CO_2 acts as a heat sink that absorbs carbonation reaction heat, so the higher the CO_2 excess, the better the cooling of the reactor. Thus, due to this phenomenon, reaction in 2:1 CO_2 analogy initiates sooner leading to extremely high temperatures after the second meter of the reactor (~890 °C) in comparison with 3:1 (Figures 5b), in which maximum temperature ranges in more reasonable and allowable values (~850 °C). In case of 3:1 CO_2 excess, reaction is accomplished in a wider reactor zone, covering the most of the reactor's length (Figure 5c). Even if the CO_2 affects significantly the response of the process, the final sorbent conversion reaches approximately the same value both in the 2:1 (X_{CaO} ≈ 0.37) and in the 3:1 ratio respectively (X_{CaO} ≈ 0.39) (Figure 5a). Velocities of gas and solid phase follow a rapid increase due to the abrupt temperature raise, and then decreases linearly in a constant way (Figure 5d).

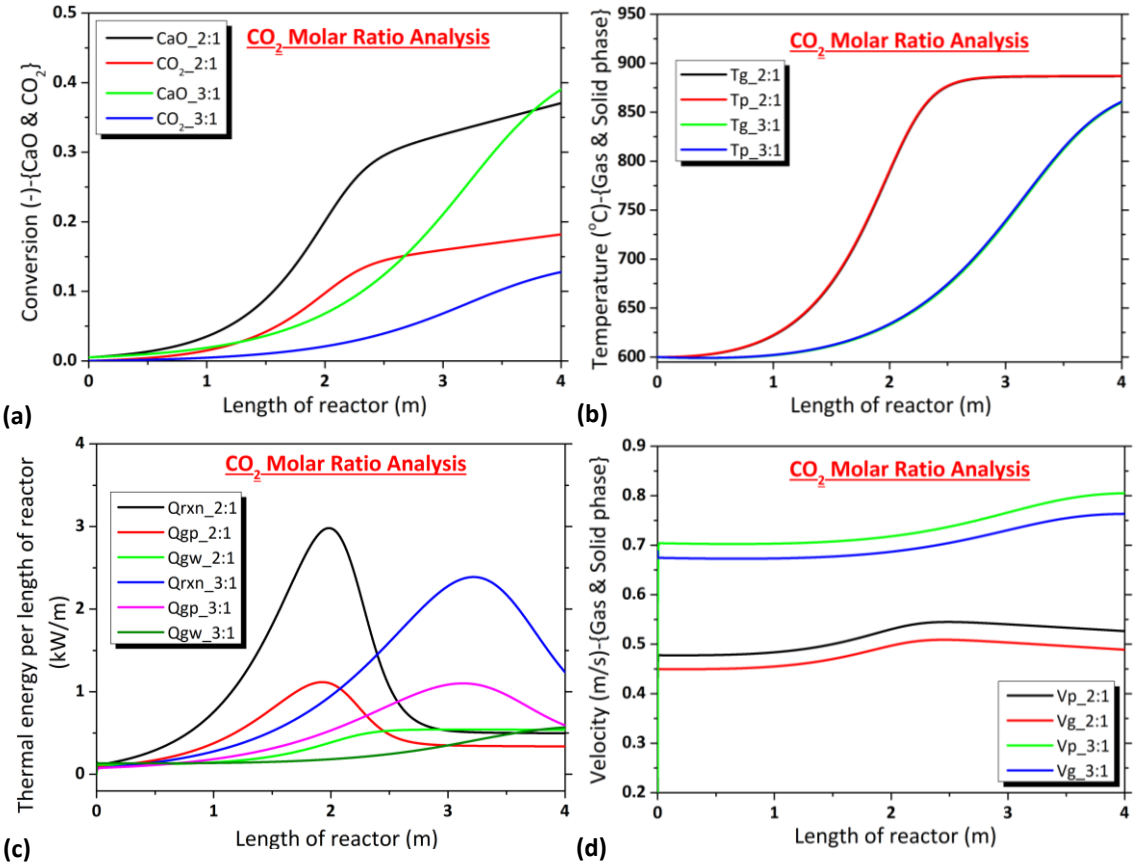

Figure 5. Comparison of the crucial process variables profiles under two different CO_2:CaO molar ratio analogies (2:1; 3:1) respect to the: (a) Conversion of CaO and CO_2, X_{CaO}, X_{CO2}; (b) Temperatures of gas and solid phase, T_g, T_s; (c) Thermal energy produced due to reaction, transferred from solid to gas phase and transferred from gas phase to wall per length of reactor, Q_{rxn}, Q_{gp}, Q_{qw}; (d) Velocity of gas and solid phase (v_g, v_p).

As long as CO_2 excess further increases, a hindering effect in the reaction initiation is occurred. The very high CO_2 flow in both cases (Figure 6), prevents carbonation initiation as temperature of the reactor does not boosts enough to enhance reaction rate. Also, due to the high CO_2 excess, the cooling rate of the reactor is such high that almost reactors' temperature maintains steady (~600-650 °C) (Figure 6b). Due to the severe initiation delay, reaction rate starts increasing almost 1.5 meter and 2 meters from the start for both cases respectively (Figure 6c). By this high CO_2 excess operation regime, sorbent conversion diminishes further, and reaches almost 22% in case of 4:1 CO_2:CaO and 11% in case of 5:1 (Figure 6a). Sorbent conversion increases with CO_2 excess until a critical CO_2 excess value, and then a reverse trend is observed as a very high CO_2 excess inhibits reaction initiation resulting in poor sorbent conversions (Figure 5,6a). Due to small temperatures variation in these cases, velocities profiles of both gas and solid phase tends to be mild enough to presumed constant (Figure 6d).

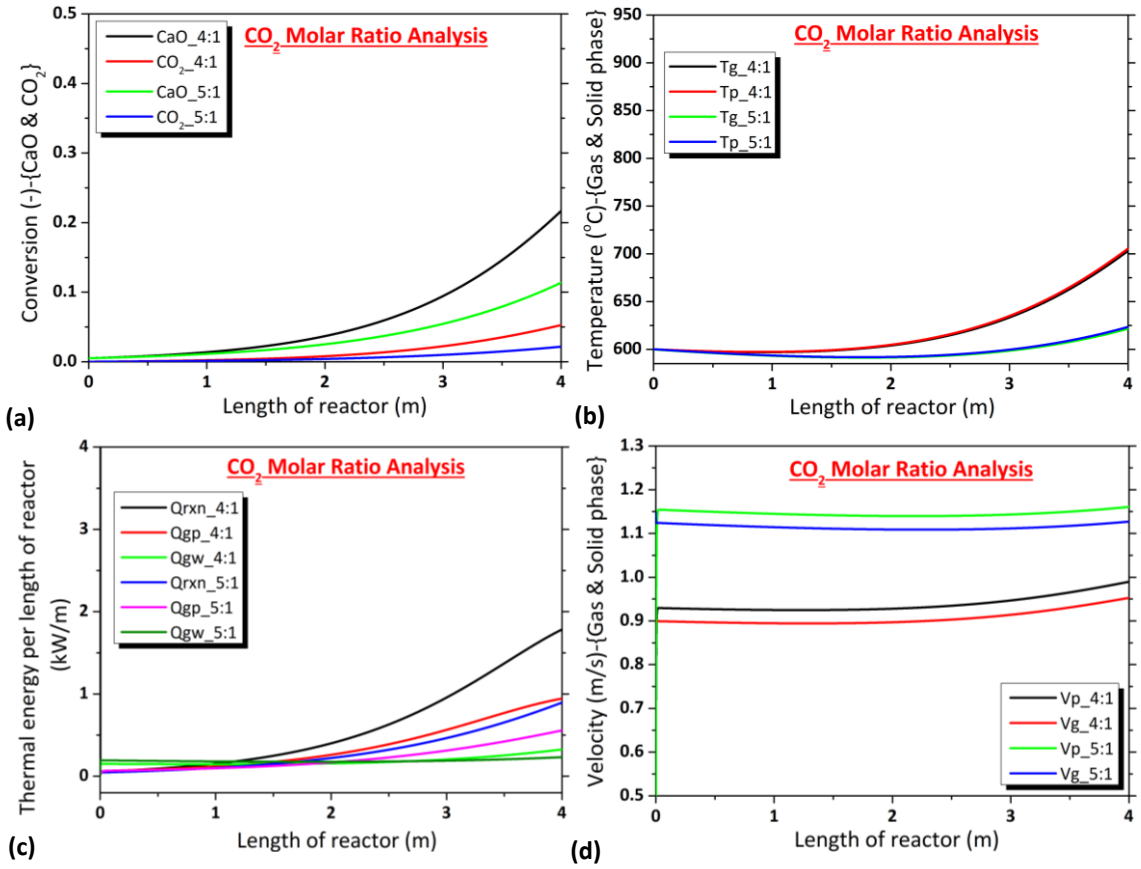

Figure 6. Comparison of the crucial process variables profiles under the four different CO_2:CaO molar ratio analogies (4:1; 5:1) respect to the: (a) Conversion of CaO and CO_2, X_{CaO}, X_{CO2}; (b) Temperatures of gas and solid phase, T_g, T_s; (c) Thermal energy produced due to reaction, transferred from solid to gas phase and transferred from gas phase to wall per length of reactor, Q_{rxn}, Q_{gp}, Q_{qw}; (d) Velocity of gas and solid phase (v_g, v_p).

4.1.3. Sorbent conversion analysis with crucial process variables

In this section, a sorbent conversion study is conducted with respect to different crucial variables. In particular, the scope of this section is to investigate the effect of the initial reactant's temperature, T_{in}, carbonator wall temperature, T_w, CO_2 molar ratio excess and particle size, d_p in the sorbent conversion profile along the reactor. Similar with the previous cases, initial reactant's temperature, T_{in} is set at 600 °C, wall temperature T_w, at 500 °C, while CO_2 to CaO molar ration is studied within a wide range of 1:1 to 5:1. Finally, the impact of the size of the particles is parametrically studied within a range of very fine particles (5 μm) and coarse particles (170 μm) that constitutes potential particles sizes for downers reactors applications [8].

In the figure below, (Figure 7), the meaningful impact of different process variables in the sorbent conversion is illustrated. Firstly, as analyzed previously, reactants inlet temperature has an important influence in sorbent conversion. The lower the inlet temperature, the slower the carbonator reaches equilibrium temperature, the slower reaction rate diminishes, so the higher the sorbent conversion. In these cases, sorbent conversion ranges between 19.7-30.3% (Figure 7a). Moreover, wall temperature, has a significant role in the final sorbent conversion (23-37.3%), as the lower the temperature, the better the cooling rate of the reactor. Thus, as reaction rates determines proportionally to the cooling rate, maximum conversion is achieved with the lower wall temperature (Figure 7b). Finally, parametric analysis of particles diameter does not seem to affect at all final sorbent conversion, albeit it slightly affects the trajectory due to different solid phase velocity variation caused by the different diameter sizes. It is worthy to

be mentioned that in the present model, reaction rate constant is not affected by the size of the particles. This state may be inconsistent with the reality as it is reasonable that with small particles diameters (i.e. d_p = 5 μm), mass transfer phenomena will be negligible, while in coarse particles (i.e. d_p >100 μm) mass transfer limitations due to diffusion will be considerable enough to affect reaction rate. In this deliverable, as reaction kinetics have been emerged by experimental procedures of mean particles diameter values, (45-75 μm), simulations within this range of diameters are assumed accurate in terms of the kinetics.

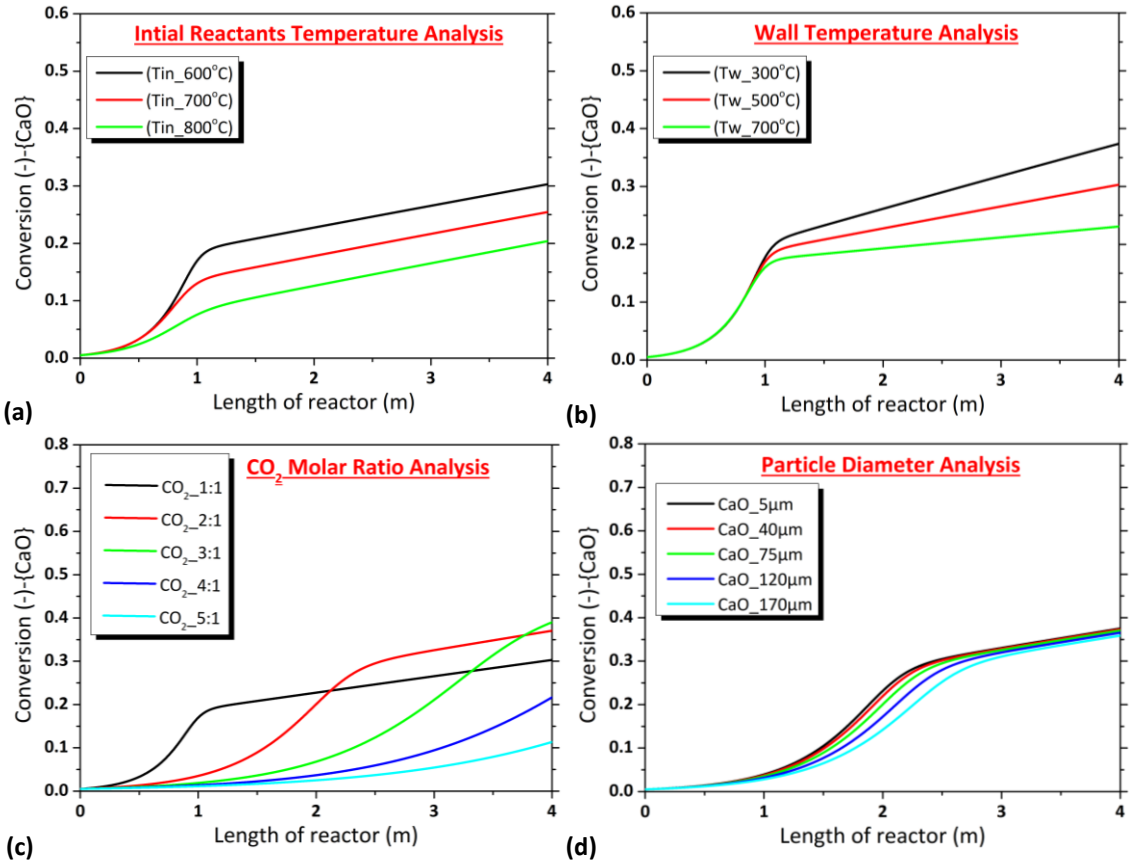

Figure 7. Comparison of the CaO conversion profile under crucial process variables: Inlet reactants temperature, T_{in}, reactor's wall temperature, T_w, particles diameter, d_p and CO_2 mass flow rate, m_{CO2} respect to the: (a) T_w (T_w = 500 °C), m_{CO2} (m_{CO2} = 10 kg h^{-1}) and d_p (d_p = 75 μm); (b) T_{in} (T_{in} = 600 °C), m_{CO2} (m_{CO2} = 10 kg h^{-1}) and d_p (d_p = 75 μm); (c) T_{in} (T_{in} = 600 °C), T_w (T_w = 500 °C) and d_p (d_p = 75 μm); (d) T_{in} (T_{in} = 600 °C), T_w (T_w = 500 °C) and m_{CO2} (m_{CO2} = 20 kg h^{-1}).

4.2. Reactor performance under low maximum sorbent conversion and "slow" kinetics

On the other hand, simulation activities of carbonator operation within a low maximum sorbent conversion, (Xk = 0.150) is mandatory to be performed, as this state represents the operation of the system under the residual sorbent conversion (i.e., after 10 cycles of calcination/carbonation residual conversion of natural limestones diminishes usually under 30%, D.2.1, [19], [22]–[24]). SOCRATCES prototype plant operation is going to be performed in these conditions, so a preliminary evaluation of carbonator performance constitutes a prerequisite both for the understanding of the prototype operation and for the integration of the model in already existed up-scaled studies for CSP-CaL units [25]–[27].

As resulted from the previous sections, initial reactant's temperature, T_{in}, is reasonable to be fixed at the lower value of 600 °C in which kinetic measurements are relatively accurate, and particle diameter, d_p, to be set at 75 μm as a representative size of the particles that have been kinetically studied (1st WP2 internal report and D2.1). Also, temperature of the wall, T_w, is set at

500 °C as an average value between 300 and 700 °C studied in the previous sections. Thus, in the next section, the CO_2 molecular excess is examined subjected to different process variables, such as: sorbent conversion, X_{CaO}, gas phase temperature, T_g, energy produced due to reaction per length of reactor, Q_{rxn} and solid phase velocity profile, v_p.

4.2.1. CO_2 excess analysis

In the next figure (Figure 8), the impact of CO_2 excess in different carbonator variables is examined. As seen, a different sorbent conversion profile is acquired as the CO_2 excess increases from 1:1 to 3:1 (Figure 8a). Specifically, the higher the CO_2 excess, the higher the solid phase velocity (Figure 8d), and thus the sooner the solid phase exits the reactor. For that reason, a small decrease in the final sorbent conversion is observed (15→13.5%) when CO_2 excess approaches the maximum value. Also, due to high CO_2 excess, surplus thermal energy is absorbed and transferred to the wall. So, temperature profile of gas phase decreases significantly as CO_2 excess increases (Figure 8b). As CO_2 excess increases, maximum temperature of gas phase (carbonator temperature) decreases from ~788 °C (CO_2_1:1) to ~660 °C (CO_2_3:1). Moreover, reaction is accomplished in a broaden reactor zone as CO_2 excess increases, shaping a more uniform profile for the produced thermal energy (Q_{rxn}) due to reaction (Figure 8c).

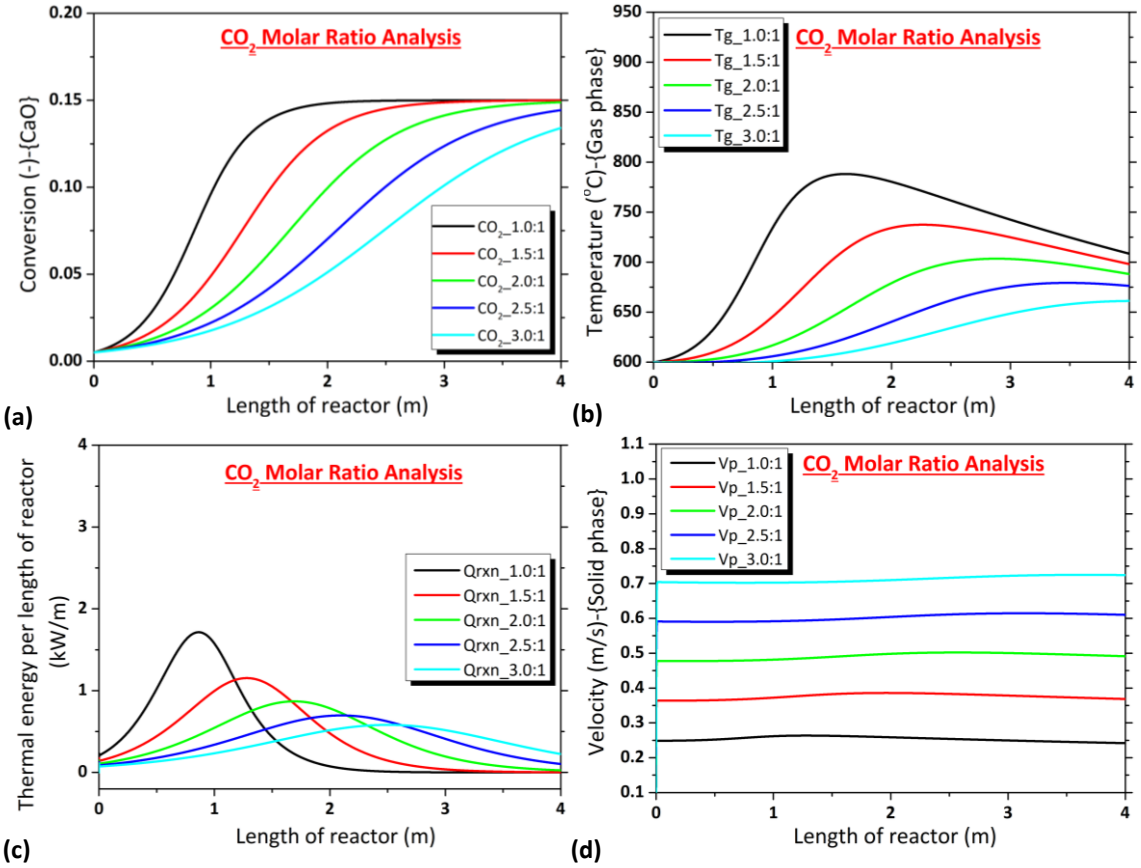

Figure 8. Comparison of the crucial process variables profiles under five different CO_2:CaO molar ratio analogies (1:1; 1.5:1; 2:1; 2.5:1; 3:1) respect to: (a) Conversion of CaO, X_{CaO}; (b) Temperatures of gas phase, T_g; (c) Thermal energy produced due to reaction per length of reactor, Q_{rxn}; (d) Velocity of solid phase (v_p).

4.3. Reactor performance under high maximum sorbent conversion and "fast" kinetics

4.3.1. CO_2 excess analysis

In this section, the carbonator model is being solved again but for different kinetics compared with the previous one and for high maximum sorbent conversion (Xk = 0.691). The kinetic model that has been used in this section was acquired by deliverable D2.1 and AUTH studies and is characterized faster in comparison with the kinetics used in previous sections (1st WP2 internal report). In this stage of the model development, it is reasonable to obtain model solutions under different kinetics studies to verify model capabilities. Later, it is intended to end-up with a unique kinetic model that describes best carbonation reaction.

Like previous, a gradual sorbent conversion raise is observed with CO_2 excess, (Figure 9a), with the maximum conversion (~52%) to be acquired in 4:1 CO_2 analogy. For larger analogies, sorbent conversion starts decreasing, as residence time of solids are reducing significantly enough to affect conversion due to higher particle velocities (Figure 9d). Moreover, carbonator temperature profile reaches almost equilibrium temperature (~890 °C), and alters considerably with CO_2, as the higher the CO_2 excess the more gas phase acts as a heat sink that absorbs heat o reaction. Therefore, the higher the CO_2 excess, the lower the carbonator temperature profile (Figure 9b). Furthermore, the higher the CO_2 excess, the wider the carbonation reaction zone (Figure 9c).

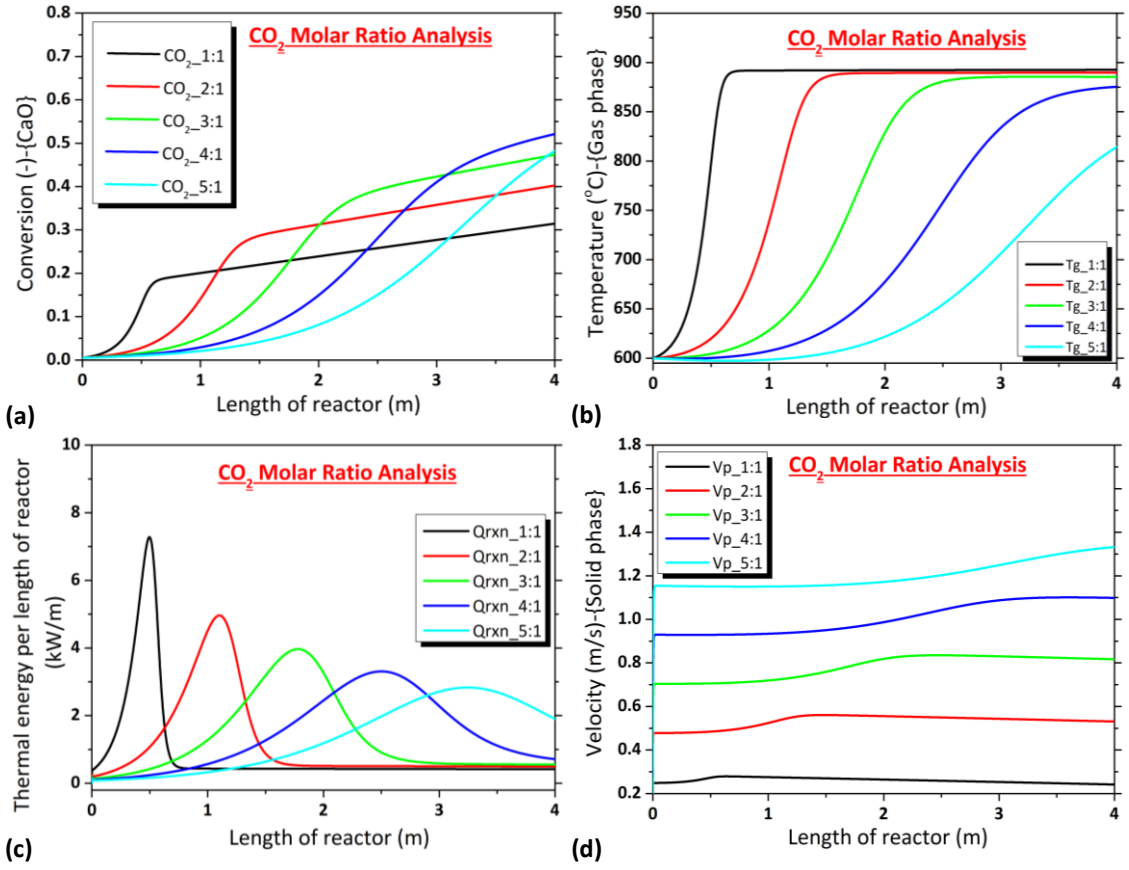

Figure 9. Comparison of the crucial process variables profiles under five different CO_2:CaO molar ratio analogies (1:1; 2:1; 3:1; 4:1; 5:1) respect to: (a) Conversion of CaO, X_{CaO}; (b) Temperatures of gas phase, T_g; (c) Thermal energy produced due to reaction per length of reactor, Q_{rxn}; (d) Velocity of solid phase (v_p).

4.4. Reactor performance under low maximum sorbent conversion and "fast" kinetics

4.4.1. CO_2 excess analysis

Similarly, in this section, the same carbonator performance analysis is conducted, with fast kinetics (1st WP2 internal report) and for low maximum sorbent conversion (Xk = 0.15). The same trends for the variable's profiles are observed also, with the maximum sorbent conversion (X_{CaO} = 15%) to be easily achieved in all cases, but with significant delays (Figure 10a). The higher the CO_2 excess, the higher the solid phase velocity (Figure 10d) and so the sooner the solids exits the reactor. Also, carbonator temperature profile deviates meaningful from the previous case (section 4.4.1), as lower sorbent conversion results in lower carbonator temperatures due to lower produced energy (Figure 10b). As shown, maximum temperatures of reactor are decreased significantly with CO_2 excess ranging between 680-807 °C.

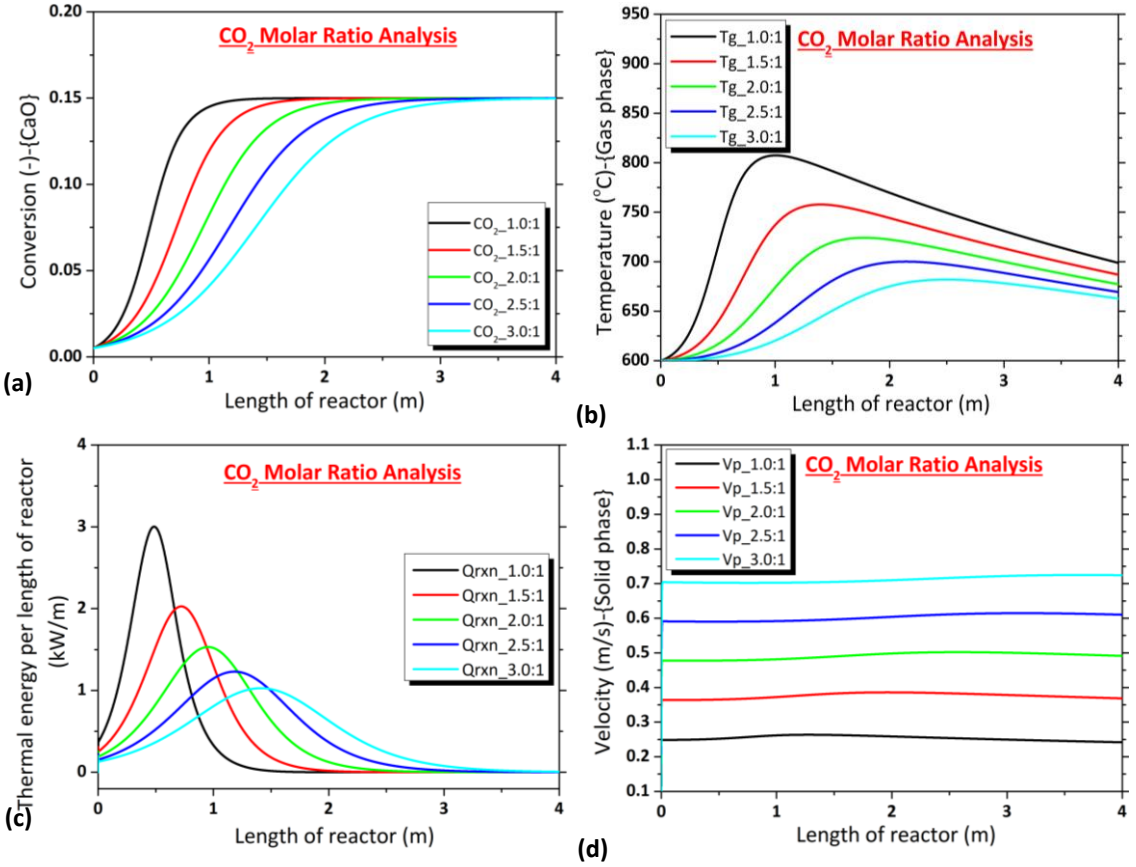

Figure 10. Comparison of the crucial process variables profiles under five different CO_2:CaO molar ratio analogies (1:1; 2:1; 3:1; 4:1; 5:1) respect to: (a) Conversion of CaO, X_{CaO}; (b) Temperatures of gas phase, T_g; (c) Thermal energy produced due to reaction per length of reactor, Q_{rxn}; (d) Velocity of solid phase (v_p).

4.5. Carbonator thermal analysis

In the last section, a carbonator thermal analysis study is performed for both kinetic models ("slow" and "fast" kinetics) and for both maximum sorbent conversions (Xk = 0.691 and 0.15). In the graph below, (Figure 11), the total produced heat of reaction Q_{rxn_tot}, and the total transferred heat from gas phase to the wall, Q_{gw_tot} is depicted. As seen, the total produced heat is initially increasing with CO_2 molar ratio and then decreases for high ratios in case of "high" sorbent conversion (Figure 11a,c). This happens, because at first, low CO_2 excess hinders carbonation completion as equilibrium temperature is easily achieved, and then in high CO_2 analogies, even if there is superfluous CO_2 to extract carbonation heat, the high solids velocities

justify the reduction of carbonation conversion and subsequently the produced heat (Q_{rxn_tot}). It is also observed that the total produced heat is greater with the "fast" kinetic model (3.45-5.35 kW) compared with the "slow" one (1.21-4.32 kW) (Figure 11a,c). On the other hand, in case of the "low" sorbent conversion, there is no considerable difference in the total produced heat (~1.62 kW) for both kinetics, as almost in all cases, carbonation conversion reaches the maximum value (X_{CaO} =15%). Regarding the total transferred thermal energy to the walls, it is highly depended on gas phase velocity. The higher the gas phase velocity, the higher the heat transfer coefficient. However, the higher the velocity, the lower the contact time of gas phase and wall. So, these criteria define in a contradictory way the heat transfer between gas phase and carbonator's wall. The latter amount of transferred heat ranges for "fast" kinetics between 1.19-1.76 kW ("high" sorbent conversion) and 0.84-1.03 kW ("low" sorbent conversion) and for "low" kinetics between 0.73-1.55 kW ("high" sorbent conversion) and 0.68-0.96 kW ("low" sorbent conversion).

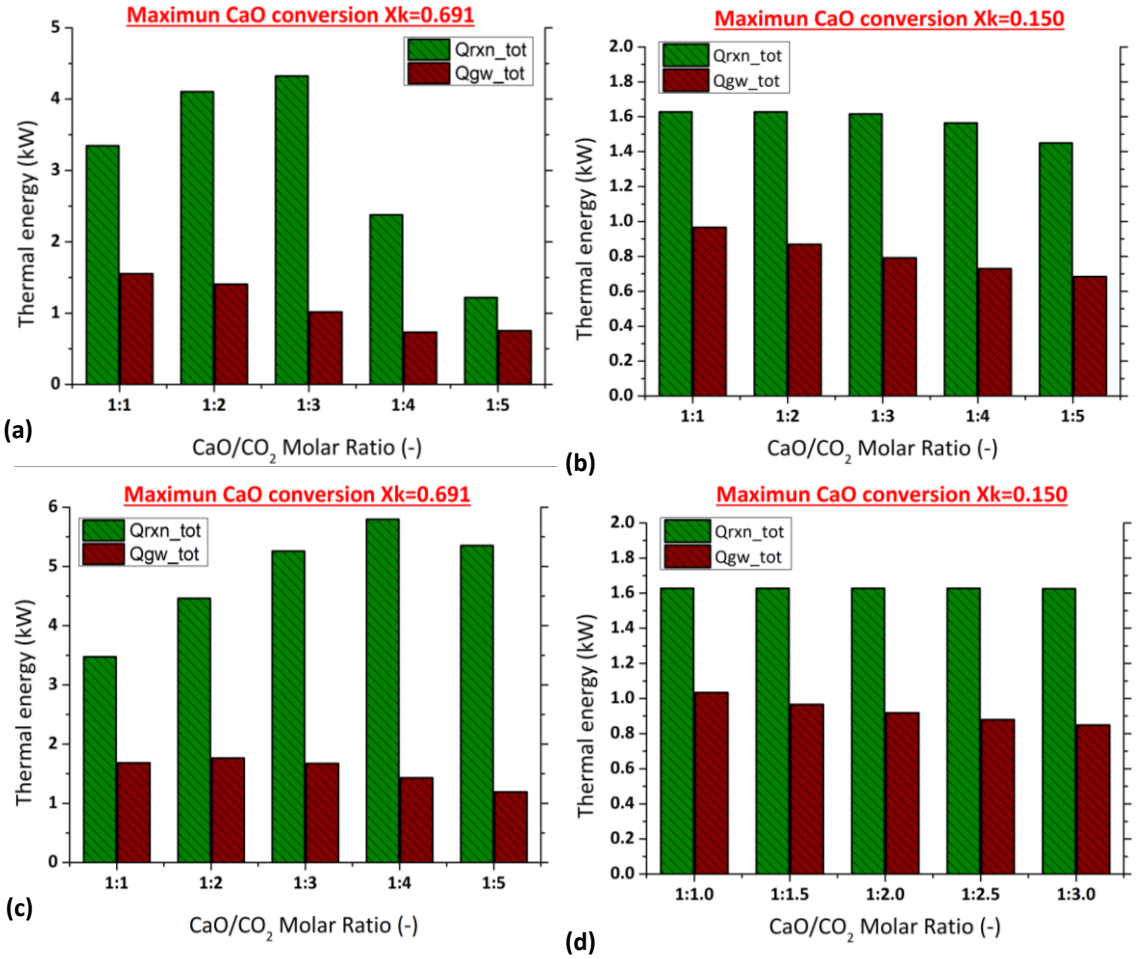

Figure 11. Comparison of the total produced energy due to reaction and the total transferred energy to the wall (Q_{rxn_tot}; Q_{gw_tot}) under two different CaO maximum conversions and two different kinetics: (a) Maximum conversion of CaO, Xk = 0.691, carbonation kinetics 1st WP2 internal report; (b) Maximum conversion of CaO, Xk = 0.150, carbonation kinetics 1st WP2 internal report; (c) Maximum conversion of CaO, Xk = 0.150, carbonation kinetics D2.1; (d) Maximum conversion of CaO, Xk = 0.150, carbonation kinetics D2.1.

5. 1-D CARBONATOR REACTOR MODEL (ZAR)

5.1. Description

The carbonator is a co-current entrained flow reactor covered with a helical pipe providing the cooling required to evacuate the heat of the exothermal carbonation reaction. The carbonator is separated in 2 tubes of 2 meters long each, placed one above the other. The cooling fluid in the upper carbonator is the same CO_2 that is later introduced as reactant, and it enters at the bottom. Moreover, the cooling fluid in the second carbonator is also CO_2, but in this case, it is introduced at the top and used in the Stirling engine for the power production.

The base case for the feed flow of CO_2 and CaO is 10.0 kg h^{-1} and 12.7 kg h^{-1}, respectively. The gaseous atmosphere in the carbonator is 100% CO_2. Pressure is constant along the carbonator (1 bar as base case).

To calculate the residence time of the gas in the carbonator, 1-D plug flow is considered. The entraining velocity in downflow for the solid is calculated through the terminal velocity and the gas velocity. The reactor has been discretized in slides of 2 cm length.

Table 18. Properties of the carbonator model.

PARTNER	ZAR	
EQUIPMENT	CARBONATOR	
SOFTWARE	EES (Engineering Equation Solver)	
SCOPE	Chemical, hydrodynamic and thermal simulations of carbonator to assess the design of the equipment and quantification of cooling requirements.	
INPUTS	METHODOLOGY	OUTPUTS
• Inlet conditions of CO_2 and CaO (T_0, P_0, $\dot{m}_{0.CO3}$, $\dot{m}_{0.CaO}$) • Inlet conditions of the cooling and stirling fluids ($T_{0,c}$, $P_{0,c}$, $\dot{m}_{0,c}$, $T_{0,s}$, $P_{0,s}$, $\dot{m}_{0,s}$) • Carbonator dimensions (L, r_{in}, r_{out}) • Particle diameter (DP)	Chemical reaction kinetics: Prout-Tompkins model from D2.1	• Flow conditions at length i (T_i, P_i, $\dot{m}_{i.CO2}$, $\dot{m}_{i.CaO}$, $\dot{m}_{i.CaCO3}$) • Conversion and reaction rate at length i (X_i, r_i) • Residence times and velocities of the solid and the gas at length i ($t_{i,s}$, , $t_{i,g}$, $v_{i,s}$, $v_{i,g}$) • Flow conditions of the cooling and stirling fluids at length i: ($T_{i,c}$, $P_{i,c}$, $\dot{m}_{i,c}$, $T_{i,s}$, $P_{i,s}$, $\dot{m}_{i,s}$) • Temperature of the carbonator at the center, inner wall and outer wall at length i (T_i, $T_{i,iw}$, $T_{i,ow}$) • Produced heat through carbonator and evacuated heats by convection and radiation at length i ($\dot{q}_i$, $\dot{q}_{i,conv}$, $\dot{q}_{i,rad}$)

5.2. Methodology

5.2.1. Carbonation kinetic model

The kinetic model is the one presented by AUTH within Deliverable 2.1 (CSIC as leader). Thus, the carbonation reaction is described by Equation 50, which gives the conversion of CaO as a function of time:

$$X(t) = \frac{X_k}{1 + e^{-r(t-t_0)}} \tag{50}$$

where X_k is the conversion at the end of the reaction-controlled phase (assumed as 0.691 for fresh CaO and 0.133 for recycled CaO) and t_0 the time taken to reach a $X_k/2$ conversion (assumed as 1.515 s). In addition, the reaction rate r is given by Equation 2 as a function of temperature and CO_2 partial pressure:

$$r = a_2 \cdot e^{\left(-\frac{\Delta S_2^0}{R} - \frac{E_1}{RT}\right)} \cdot \left(\frac{P}{P_{eq}} - 1\right) \tag{51}$$

where a_2 is 74900 s^{-1}, ΔS_2^0 is -68 J mol^{-1} K^{-1} and E_1 is 180 kJ mol^{-1}. Besides, $P_{eq} = A \cdot \exp(-\alpha/T)$, where A is 4.083 · 10^7 atm, and α is 20474 K.

The kinetic model allows computing the mole flow of each component as a function of time. Therefore, to characterize the carbonator based on its dimensions, it is required to know how long the solid and the gas are interacting as they flow down through the reactor.

5.2.2. Residence time for the solids

The time of interaction between the solid and the gas is limited to the residence time of the solid in the carbonator since its terminal velocity must be also accounted. For those flows with Reynolds lower than 2 and small size particles, the following Equation 52 may be applied for the downward velocity of single particles, v_s, (concentration of particles is assumed diluted) [28]:

$$v_s = v_{s,i} \cdot e^{-bt_s} + \left(v_g + v_t\right) \cdot (1 - e^{-bt_s}) \tag{52}$$

where $v_{s,i}$ is the initial velocity of the solid, v_g is the velocity of the gas phase, and v_t is the terminal settling velocity of the particle in a static fluid. The parameter b, and the velocity v_t are given by Equation 53 and Equation 54:

$$b = \frac{18\mu}{\rho_s d_p^2} \tag{53}$$

$$v_t = \frac{\left(\rho_s + \rho_g\right) d_p^2 g}{18\mu} \tag{54}$$

where μ is the viscosity of the gas, ρ_s is the density of the solid, ρ_g is the density of the gas, d_p is the diameter of the solid particles, and g the gravity.

The integration of Equation 52 provides the relationship between the carbonator length and the residence time of the solids (Equation 55).

$$L = \int_0^{t_{s,L}} v_s dt_s = \frac{v_{s,i}}{b}(1 - e^{-bt_s}) + \left(v_g + v_t\right) \cdot \left(t_s - \frac{1 - e^{-bt_s}}{b}\right) \tag{55}$$

It can be assumed that v_g and μ are constants in the interval of integration for the case of study. Thus, this can be directly solved by the EES software to compute the residence time of the solid as a function of the length, what will allow determining the mole flows along the reactor as a function of the distance from the entrance.

5.2.3. **Plug flow model (1-D) for the gas**

The residence time of the gas is given by Equation 56:

$$t_g = \int_0^{V_c} \frac{\pi r_{in}^2}{\dot{V}} dL \tag{56}$$

where r_{in} is the inner radius of the carbonator, $\dot{V}$ is the volumetric flow rate, and V_C the carbonator volume. Moreover, $\dot{V}$ is the product of the gas velocity multiplied by the cross-sectional area of the reactor, which in the study case must be corrected by subtracting the area occupied by the solid. The variation in the effective cross-sectional area along the reactor may be neglected as $CaCO_3$ is produced when CaO is consumed.

Besides, it is assumed that the pressure inside the reactor remains constant. Hence, the volumetric flow rate is given by Equation 57, according to the ideal gas law:

$$\dot{V}_{L2} = \frac{(1 - X_{L2}) \cdot T_{L2}}{T_{L1}} \dot{V}_{L1} \tag{57}$$

The residence time of the gas, through a length L_i in which $\dot{V}_{Li}$ can be considered constant will be $t_{g(L1)} = L_i \cdot S_{eff}/\dot{V}_{Li}$.

5.2.4. **Heat transfer model**

The carbonator is covered with a spiral pipe acting as cooling jacket. The following steps are taken to compute the heat transfer from the cloud of gas and particles to the cooling fluid. First, an energy balance inside the reactor is computed for each slice of reactor (from length L_{i-1} to length L_i) by Equation 58:

$$\sum_j Cp_j \cdot \dot{n}_{j,L_i} \cdot \left(T_{L_i} - T_{L_{i-1}}\right) = -\Delta H_r \cdot \left(\dot{n}_{CaCO3,L_i} - \dot{n}_{CaCO3,L_{i-1}}\right) - \dot{q}'_{L_i} \cdot (L_i - L_{i-1}) \tag{58}$$

where Cp_j and $\dot{n}_{j,}$ are the specific heat and mole flow of component j, respectively, T is the temperature of the cloud of gas and particles (which is assumed homogeneous inside the carbonator), ΔH_r is the heat of reaction (-178 kJ mol^{-1}), and $\dot{q}'_{L_i}$ is the heat flow throughout the inside wall of the carbonator per unit of length. The latter accounts for radiation and convection, in the form of Equation 59:

$$\dot{q}'_{L_i} = \dot{q}'_{rad,L_i} + \dot{q}'_{conv,L_i} \tag{59}$$

$$\dot{q}'_{rad,L_i} = \frac{\varepsilon_w}{\alpha_{g+p} + \varepsilon_w - \alpha_{g+p} \cdot \varepsilon_w} \cdot \sigma \cdot (\varepsilon_{g+p} \cdot T_{L_i}^4 - \alpha_{g+p} \cdot T_{iw,L_i}^4) \cdot 2\pi r \tag{60}$$

$$\dot{q}'_{conv,L_i} = h_{g,L_i} \cdot \left(T_{L_i} - T_{iw,L_i}\right) \cdot 2\pi r \tag{61}$$

Where α_{g+p} and ε_{g+p} are the absorptivity and emissivity of the gas-particle mixture, ε_w the emissivity of the carbonator wall, σ is the Boltzmann's constant, T_{iw} is the temperature of the inner wall of the carbonator, r the inner radius of the carbonator, and h_g the convective coefficient.

The model for the calculation of the absorptivity and emissivity of the gas-particle mixture is borne out of the VDI Heat Atlas, Part K [29]. The total emissivity of a gas-particle mixture can be described as

$$\epsilon_{g+p} = (1 - \beta)\left(\frac{1 - \exp\left(-\Phi_{emi,g+p}\right)}{1 + \beta \exp\left(-\Phi_{emi,g+p}\right)}\right) \tag{62}$$

where

$$\gamma = \sqrt{1 + \frac{2\bar{Q}_{bsc}}{\bar{Q}_{abs}}} \tag{63}$$

$$\beta = \frac{\gamma - 1}{\gamma + 1} \tag{64}$$

$$\Phi_{emi,g+p} = \left(\bar{Q}_{abs} A L_p + K_{emi,g}\right) l_{mb} \gamma \tag{65}$$

In a similar manner the absorptivity can be calculated:

$$\alpha_{g+p} = (1 - \beta)\left(\frac{1 - \exp\left(-\Phi_{abs,g+p}\right)}{1 + \beta \exp\left(-\Phi_{abs,g+p}\right)}\right) \tag{66}$$

where

$$\Phi_{abs,g+p} = \left(\bar{Q}_{abs} A L_p + K_{abs,g}\right) l_{mb} \gamma \tag{67}$$

L_p is the particle loading, in kg m^{-3}. The parameter l_{mb} is the mean beam length of radiation within the relevant geometry. A is the specific surface area of the particles.

The determination of particle absorption and scattering coefficients Q_{abs} and Q_{bsc} is performed graphically, and limestone is included on the graph in the Heat Atlas. The mean particle diameter d_p is measured experimentally, or can be calculated from the surface area and density of the particles by

$$d_p = \frac{3}{2\rho_p A} \tag{68}$$

The gas absorption and scattering coefficients are defined as

$$K_{emi,g} = -\frac{\ln\left(1 - \epsilon_g\right)}{l_{mb}} \tag{69}$$

$$K_{abs,g} = -\frac{\ln(1 - A_v)}{l_{mb}} \tag{70}$$

where ε_g is the emissivity of the gas and A_v is its absorptance. The value of ε_g varies with pressure, optical thickness and temperature. It is found using a graph in the Heat Atlas [29]. The absorptance A_v is a function of the wall and gas temperatures and the emissivity of the gas:

$$A_v = f_{p,CO_2}\left(\frac{T_g}{T_w}\right)^{0.65} \epsilon_g \tag{71}$$

The above is valid for CO_2. Note that $f_{p,CO2}$ is a pressure correction factor that at 1 bar total pressure is equal to 1.

Besides, the model for the calculation of the convective coefficient is borne out of 'Heat Transfer' by Nellis G and Klein S [30], and follows Equations 72 to 76:

$$h_{g,L_i} = \frac{Nu_{Li} \cdot k_{Li}}{2r} \tag{72}$$

$$Nu_{L_i} = 3.66 + \frac{\left(0.049 + \frac{0.020}{Pr_{Li}}\right) \cdot Gz_{Li}^{1.12}}{1 + 0.065 \cdot Gz_{Li}^{0.7}} \tag{73}$$

$$Pr_{Li} = \frac{Cp_{Li} \cdot \mu_{Li}}{k_{Li}} \tag{74}$$

$$Gz_{Li} = \frac{Re_{Li} \cdot Pr_{Li}}{L/2r} \tag{75}$$

$$Re_{Li} = \frac{4 \cdot \dot{m}_{Li}}{\pi \cdot 2r \cdot \mu_{Li}} \quad (76)$$

Where Nu is the Nusselt number, k the thermal conductivity, Pr the Prandtl number, Gz the Graetz number, μ the viscosity, Re the Reynolds number, and $\dot{m}$ the mass flow.

The temperature of the outer wall of the carbonator, T_{ow}, is computed by the formula of heat conduction through a tube wall, given by Equation 77:

$$\dot{q}'_{L_i} = \frac{T_{iw,L_i} - T_{ow,L_i}}{R_{tube} \cdot L_i} \quad (77)$$

$$R_{tube} = \frac{\ln(\frac{r_{out}}{r})}{2\pi \cdot k_{tube} \cdot L_i} \quad (78)$$

where R_{tube} is the thermal resistance of the carbonator tube, r_{out} the outer radius of the carbonator, and k_{tube} the thermal conductivity of the carbonator tube (0.025 kW m^{-1} K^{-1}).

Then, it is assumed that the temperature of the carbonator's outer wall is equal to the temperature of the cooling fluid inside the helical pipe, since the convective coefficient inside the helical pipe is two orders of magnitude greater than inside the carbonator. Thus, the following energy balance on the cooling fluid is computed, assuming that $(L_i - L_{i-1})$ is equal to the diameter of the helical pipe (Equation 79):

$$Cp_c \cdot \dot{n}_c \cdot \left(T_{ow,L_i-1} - T_{ow,L_i}\right) = \dot{q}'_{L_i} \cdot (L_i - L_{i-1}) \quad (79)$$

Where Cp_c and $\dot{n}_c$ are the specific heat and the mole flow of the cooling fluid. It should be noted that Equation 30 is valid for the first carbonator in which the cooling fluid flows from bottom to top, and therefore it is heated from position L_i to L_{i-1}, with the heat produced inside the carbonator from position L_{i-1} to L_i. For the second carbonator, the energy balance is given by Equation 80, since the cooling fluid flows from top to bottom.

$$Cp_c \cdot \dot{n}_c \cdot \left(T_{ow,L_i} - T_{ow,L_i-1}\right) = \dot{q}'_{L_i} \cdot (L_i - L_{i-1}) \quad (80)$$

Thus, the temperature along the carbonator can be computed by knowing the initial temperature of the cooling fluid.

5.3. Results

5.3.1. Base case design

The base case design to be studied is a carbonator 4 meters long and 15.24 cm (6 inches) in diameter (thickness is assumed 5 mm). The residence time of the particles is 10.73 seconds (particle diameter of 60 μm). The pressure inside is assumed 1 bar and the inlet temperature of the CO_2 and CaO is 800 °C. The initial mass flow of CO_2 is 10 kg h^{-1} and the mass flow of CaO is 12.7 kg h^{-1}. Besides, both cooling fluids enter at the middle of the carbonator, so the first reactor is cooled at counter-current and the second one at co-current. The CO_2 is considered at 25 °C at the beginning of the pre-heat and at 1 bar. The Stirling fluid is assumed a CO_2 flow of 10 kg h^{-1} at 1 bar with an inlet temperature of 25 °C. The temperature profiles and conversion are presented in the following Figure.

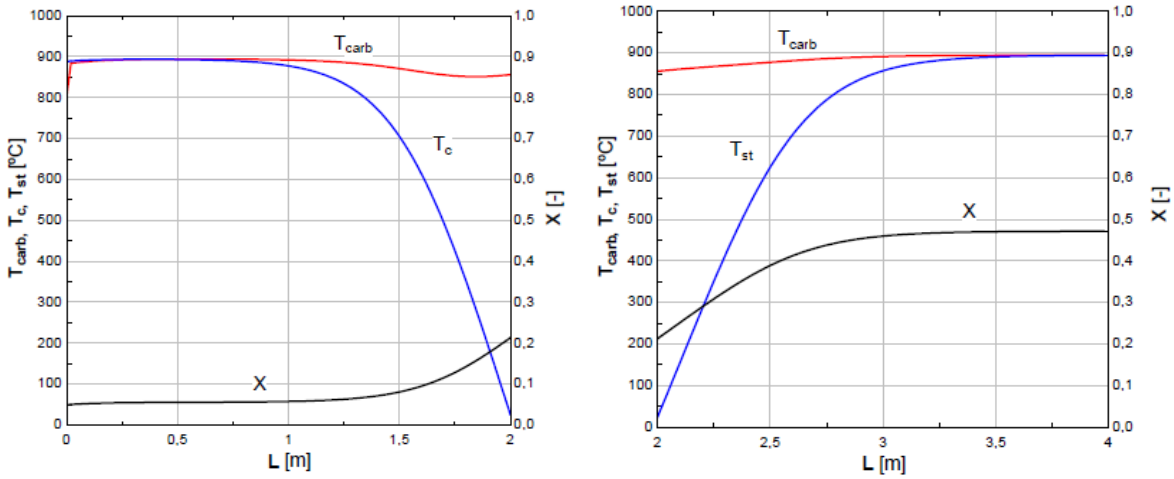

Figure 12. Temperature profiles of the carbonator (Tcarb), cooling fluid (Tc) and Stirling fluid (Tst), and the conversion (X).

The reaction is inhibited during the first 1.5 meters, and during the last meter of the carbonator. Thus, the final conversion is 47.1%. Actually, the reaction only takes place next to the entrance of the cooling fluids, which are rapidly heated. It is worth to mention that the kinetic model was developed for 1.7 bar instead for the pressure of operation of the base case design (1 bar). This leads to an error in the initial conversion, which starts at 5%. This has a strong influence in the results, which show an increment of 83 °C in the first 2 cm slice of the reactor.

Parametric analysis on CO_2 mass flow

In this parametric analysis, the mass flow of CO_2 is increased to 30 kg h^{-1} and 50 kg h^{-1} in order to better distribute the reaction and the exothermal heat along the reactor. Also, it is increased the CO_2 mass flow of the Stirling fluid.

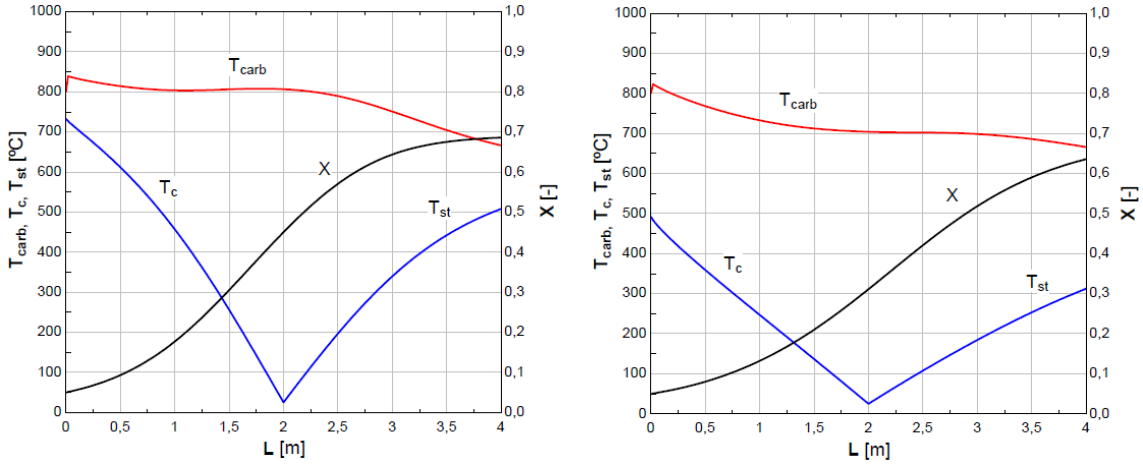

Figure 13. Temperature profiles of the carbonator (Tcarb), cooling fluid (Tc) and Stirling fluid (Tst), and the conversion (X). Left: 30 kg h^{-1}, Right: 50 kg h^{-1}.

It is found that the final conversion for 30 kg h^{-1} is 68.6%, and for 50 kg h^{-1} is 63.6%. Both situations allow cooling the reactor, but the latter has lower residence times and thus a smaller conversion. However, the final temperature of the Stirling fluid is not proper to produce enough power.

5.3.2. Parametric analysis on inlet temperature of cooling fluids

In order to not cool in excess the carbonator when CO_2 mass flows of 30 kg h^{-1} and 50 kg h^{-1} are introduced, a study for a greater inlet temperature for the cooling fluids is presented. This would allow reaching higher temperatures for the Stirling Engine. The conversions are slightly reduced

in comparison with the results of section 5.3.1 since the operation of the carbonator is a higher temperature. Nevertheless, the variations of the temperature profile of the carbonator are kept in a shorter range, what makes easier the operation.

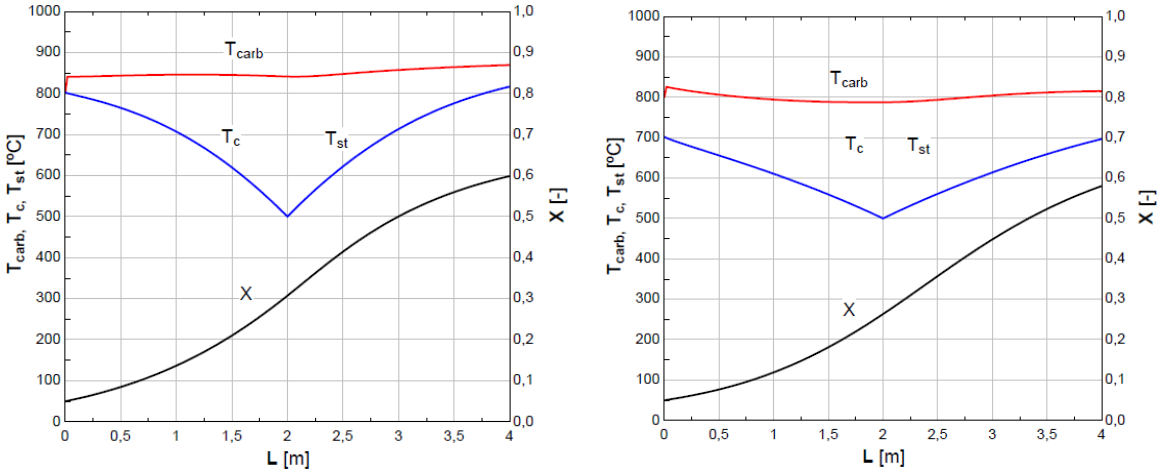

Figure 14. Temperature profiles of the carbonator (Tcarb), cooling fluid (Tc) and Stirling fluid (Tst), and the conversion (X). Left: 30 kg h^{-1} of CO_2, Right: 50 kg h^{-1} of CO_2.

It should be noted that for the 30 kg h^{-1} case the temperature of the carbonator is close or even above the temperature limit of the material of which the carbonator is made. Furthermore, in the case of 50 kg h^{-1}, the CO_2 in the helical pipe of the upper carbonator is not preheated to the required inlet temperature (800 °C).

5.3.3. The. Parametric analysis on particle diameter

Regarding the analysis of section 5.3.2, the operation with 50 kg h^{-1} of CO_2 and inlet temperatures of the cooling fluids of 500 °C leads the better results in terms of maximum carbonator temperature. Thus, in this section it is presented a study on the particle diameter (30 and 90 micron) under that configuration.

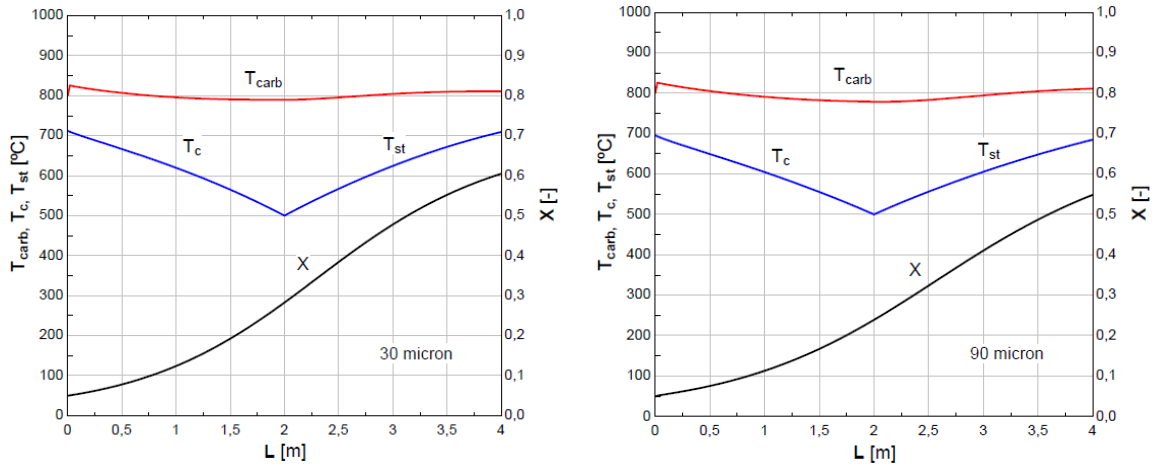

Figure 15. Temperature profiles of the carbonator (Tcarb), cooling fluid (Tc) and Stirling fluid (Tst), and the conversion (X). Operation with 50 kg h^{-1} of CO_2.

There is not a remarkable difference coming from the particle diameter used. The residence times slightly varies and so the conversion and temperatures.

5.3.4. Study for sintered CaO

In this section is used a sintered CaO, what means that the maximum residual conversion is set to 13.3%. The temperatures and mass flows of the base case design are kept unchanged. As the exothermal heat to be removed is much lower than in the base case, there is not such inhibition.

However, the base case design is not prepared for sintered CaO, as the cooling does not work properly. In one hand, it is insufficient at the beginning of the reactor, so temperatures over the technical limit are reached. In the other, it is oversized in the second half of the reactor since the carbonation reaction is already finished, and so the temperature for the Stirling engine does not allow producing any power.

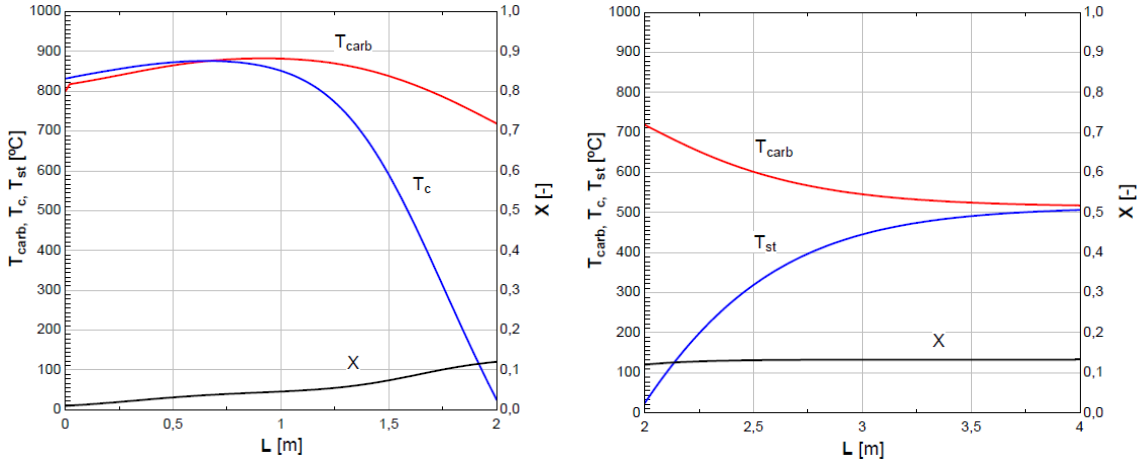

Figure 16. Temperature profiles of the carbonator (Tcarb), cooling fluid (Tc) and Stirling fluid (Tst), and the conversion (X).

5.3.5. Proposal of reducing the carbonator diameter

The proposal for design improvement is reducing the carbonator diameter in order not to require CO_2 excess in the carbonator. Thus, the proposed dimensions are 4 meters long, 6 cm in diameter, and 5 mm in thickness. The residence time of the particles is 3.76 seconds (particle diameter of 60 µm). Besides, as the kinetic model was developed under 1.7 bar, the new proposal operates also at that pressure, in order to reduce the error in the conversion at time zero. The inlet temperature of the CO_2 and CaO is 800 °C. The initial mass flow of CO_2 is 10 kg h^{-1} and the mass flow of CaO is 12.7 kg h^{-1}. Besides, both cooling fluids enter at the middle of the carbonator, so the first reactor is cooled at counter-current and the second one at co-current. The helical pipe is assumed to be 2 cm in outer diameter. The CO_2 is considered at 25 °C at the beginning of the pre-heat and at 1.7 bar. The data of the fluid for the Stirling engine is assumed a CO_2 flow of 10 kg h^{-1} at 1.7 bar and an inlet temperature of 25 °C. The temperature profiles and conversion are presented in the following Figure.

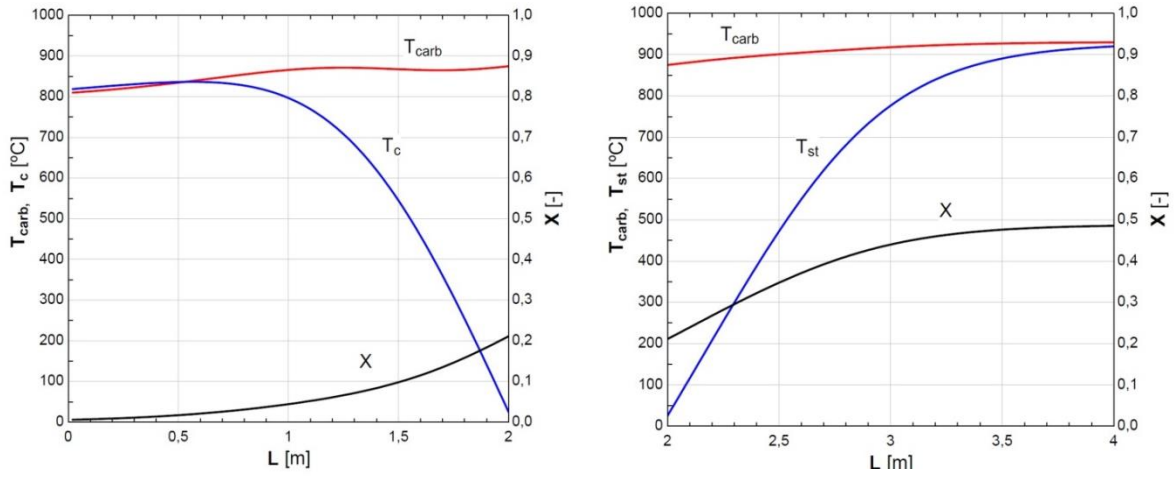

Figure 17. Temperature profiles of the carbonator (Tcarb), cooling fluid (Tc) and Stirling fluid (Tst), and the conversion (X).

The reaction is inhibited at the end of the second carbonator as temperatures about 920 °C are reached. The final conversion is 48.5%.

Parametric analysis on Stirling fluid mass flow

In this section, a parametric study on the mass flow of Stirling's fluid is performed (+0%, +50% and +100%). It can be seen that the increment in the mass flow of the Stirling fluid increases the final conversion at the end of the carbonator, as it helps not reaching the equilibrium temperature.

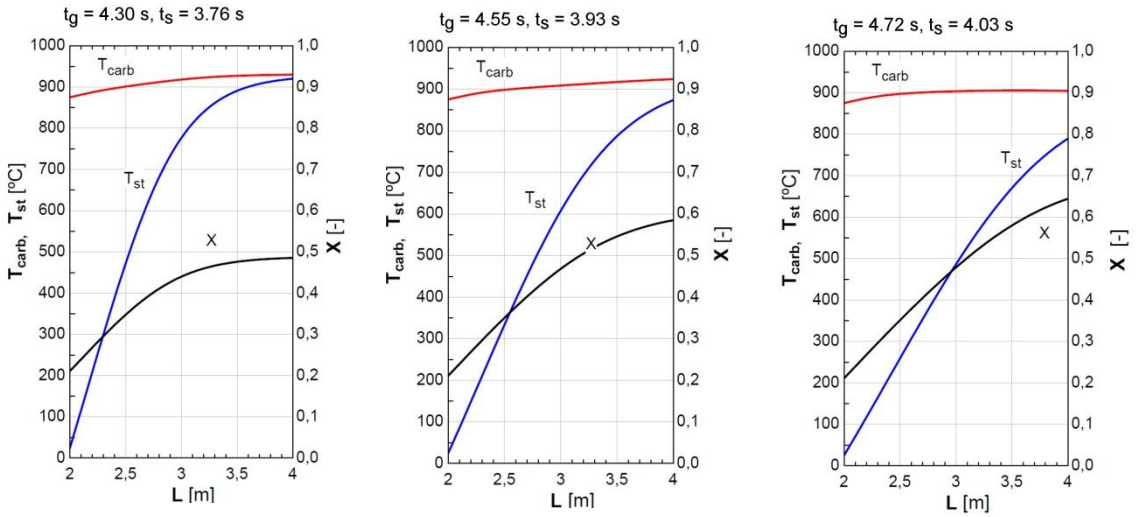

Figure 18. Temperature profiles of the carbonator (Tcarb), cooling fluid (Tc) and Stirling fluid (Tst), and the conversion (X).

Parametric analysis on particle diameter

In this section a parametric study on the diameter of the particles is presented (30 and 90 microns). It can be observed that the final conversion barely changes with the size of the particles, since the reaction is inhibited in the second carbonator due to the temperature. Moreover, there is a peak of temperature in the first carbonator that increases as the residence time rises.

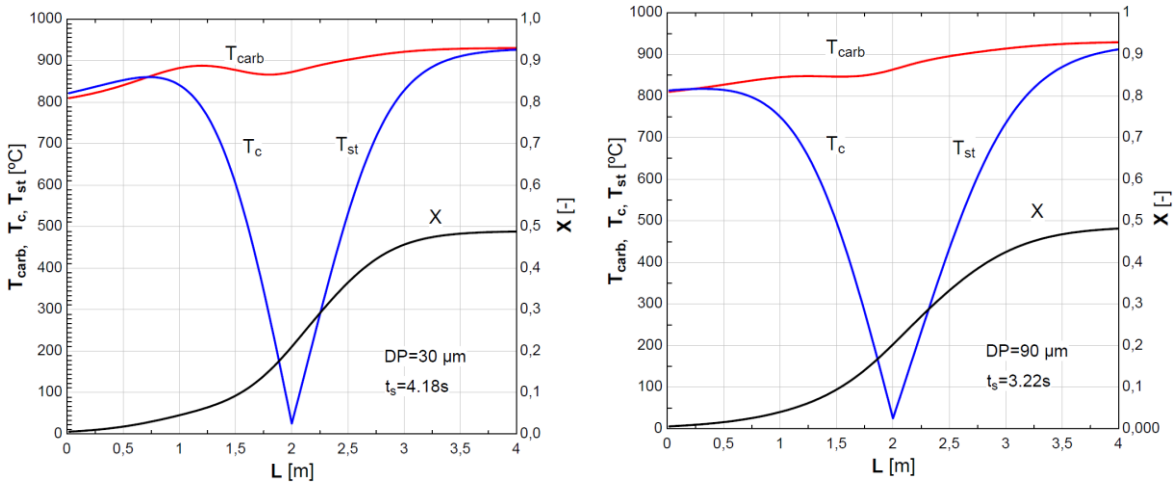

Figure 19. Temperature profiles of the carbonator (Tcarb), cooling fluid (Tc) and Stirling fluid (Tst), and the conversion (X).

Parametric analysis on carbonator diameter

In this section a parametric study on the diameter of the carbonator is presented. It can be seen that larger carbonator diameters (7 cm) only increase the residence time without incrementing the final conversion. This is because the reaction is inhibited as the cooling in the second carbonator is not enough. Besides, for lower carbonator diameters lower the reaction is cooled below the 800 °C since the residence time and the exothermal heat in the upper reactor are reduced.

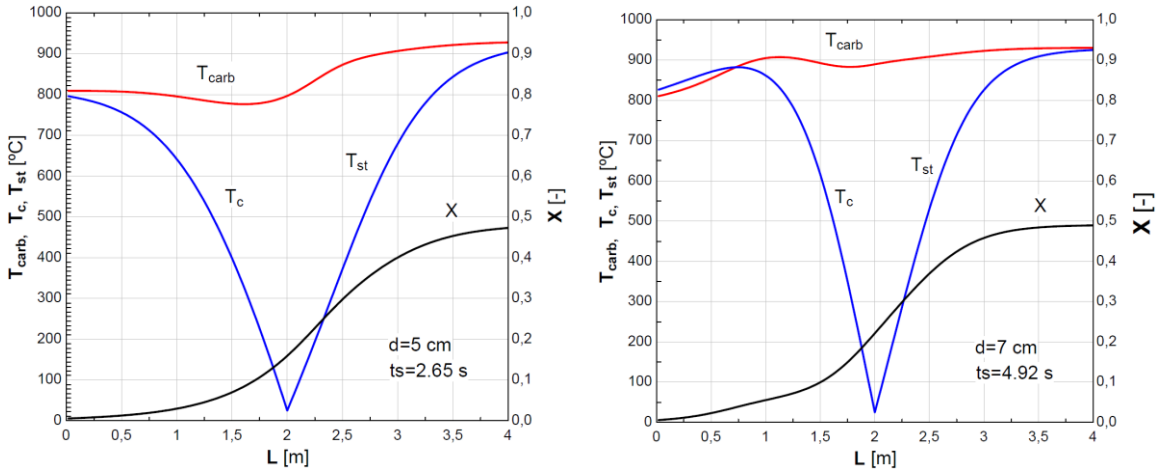

Figure 20. Temperature profiles of the carbonator (Tcarb), cooling fluid (Tc) and Stirling fluid (Tst), and the conversion (X).

Study for sintered CaO

The sintered CaO is considered to have a maximum residual conversion of 13.3%. For this case the dimensions of the carbonator are kept unchanged (4 meters long, 6 cm in diameter, and 5 mm in thickness) as well as the initial mass flow of CO_2 and CaO (10 kg h^{-1} and 12.7 kg h^{-1}, respectively). However, as the produced heat is lower, some aspects of the design have been modified to reduce the cooling: (i) The inlet temperature of the reactants is 850 °C, (ii) The inlet temperature of both cooling fluids is 500 °C, (iii) The CO_2 flow for the Stirling engine is 2.5 kg h^{-1}, (iv) The helical pipe is 4 cm in outer diameter.

The temperature profiles of both carbonators are presented under this configuration. The reaction is kept in the range 800 – 865 °C, thus avoiding inhibition. The residence time of the particles for this case is 3.1 seconds (particle diameter of 60 µm), and the residence time of the gas is 3.5 s. Velocity of the particles varies between 1.31 m/s and 1.23 m/s, while the velocity of the gas varies between 1.24 m/s and 1.09 m/s. The final conversion is 13.16%.

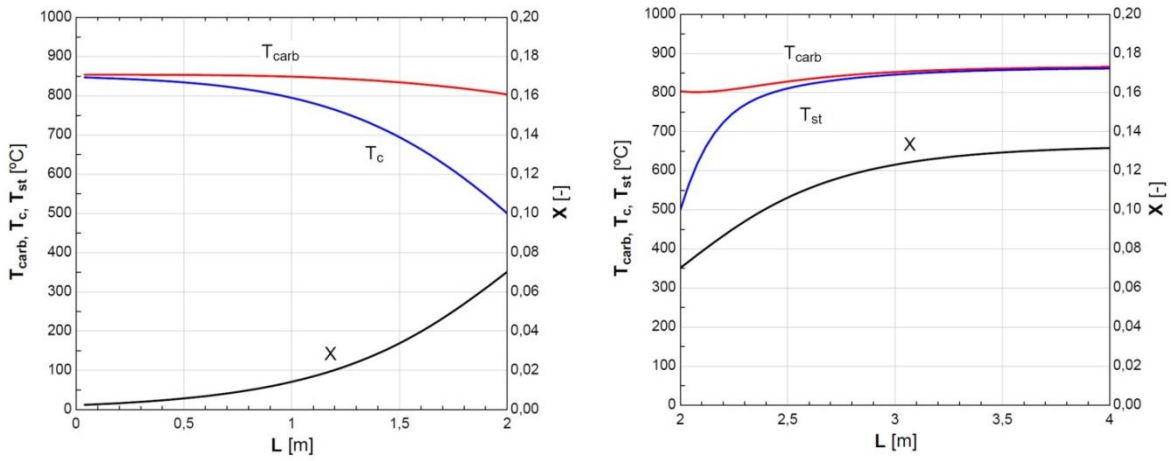

Figure 21. Temperature profiles of the carbonator (Tcarb), cooling fluid (Tc) and Stirling fluid (Tst), and the conversion (X).

6. CFD-BASED CARBONATOR REACTOR MODEL (CERTH)

6.1. Model formulation and implementation

In order to assist the understanding of the carbonation reactor dynamics in greater spatial detail and, thereby, further support model development and the reactor design, a CFD-based model of the carbonator downer reactor was developed. This model is implemented within the ANSYS Fluent computational fluid dynamics software, making use of the Discrete Phase Model contained in this software package, as well as the User Defined Function facility provided [31]. The latter facility allows user-programmed extensions to be hooked to the fluid flow and discrete phase model code and will be used primarily for incorporating, in the next step from the work presented, the carbonation reaction in the CFD-based model of the reactor.

A simplified geometric representation of the downer reactor is used as the basis of the CFD model in order to maintain computational tractability while considering the following extensive set of model features:

- fluid phase: axisymmetric flow with (optionally) swirl
- k-ε turbulence model
- compressible ideal gas fluid model
- entrained CaO solid phase motion by Langrangian particle tracking
- two-way coupling of entrained CaO solids and the flow field
- two-way interaction of the CaO solids and turbulence
- multiple reactor wall zones of prescribed temperature
- approximation of CaO solids and CO_2 reactants injections by a combination of axial and radial/tangential inlets
- uniform or prescribed feed particle size distribution
- dynamic particle size tracked on a particle-by-particle basis
- gravity in particle forces and in flow buoyancy effects

The simplified geometry employed, which can be seen in Figure 22, is discretised by a Cartesian gird with a resolution (cell size) of 2 mm. Other resolutions are possible depending on requirements, subject to the constrain that wall-adjacent grid cells are large enough to contain the laminar sublayer, as required for proper function of the turbulence model employed.

The CaO solids motion is computed by tracking individual particles subject to the action of deterministic forces (here, aerodynamic drag and gravity) as well as stochastic forces (i.e. incl. a random component) due to the effect of turbulent eddies. Particle thermal history is also tracked on a particle-by-particle basis along the particle trajectory. Conversely, the effect of the entrained solid particles on the fluid flow is also computed. The coupling of the solids' effect on the flow and temperature fields is conveyed through source terms which are calculated by applying conservation laws (momentum, energy) to the particle passage through each grid cell. The conservation of mass is treated in an identical manner when chemical reactions (that consume or emit gaseous material) are implemented. Chemical reaction dynamics are not currently implemented in the CFD-based model of the carbonator, however, the user-defined functions that will host the chemical kinetics implementation have been hooked to the flow solver in order to ensure that a user-extension functional interface is in place. In addition to coupling the reaction kinetics, user-defined extensions are needed for tracking the particle composition and size as $CaCO_3$ material accumulates on the shrinking CaO cores. As a first approximation – considering that the currently presented (initial) model does not yet account for the carbonation reaction − the physical properties of CaO are used in the current version of the CFD-based carbonator model.

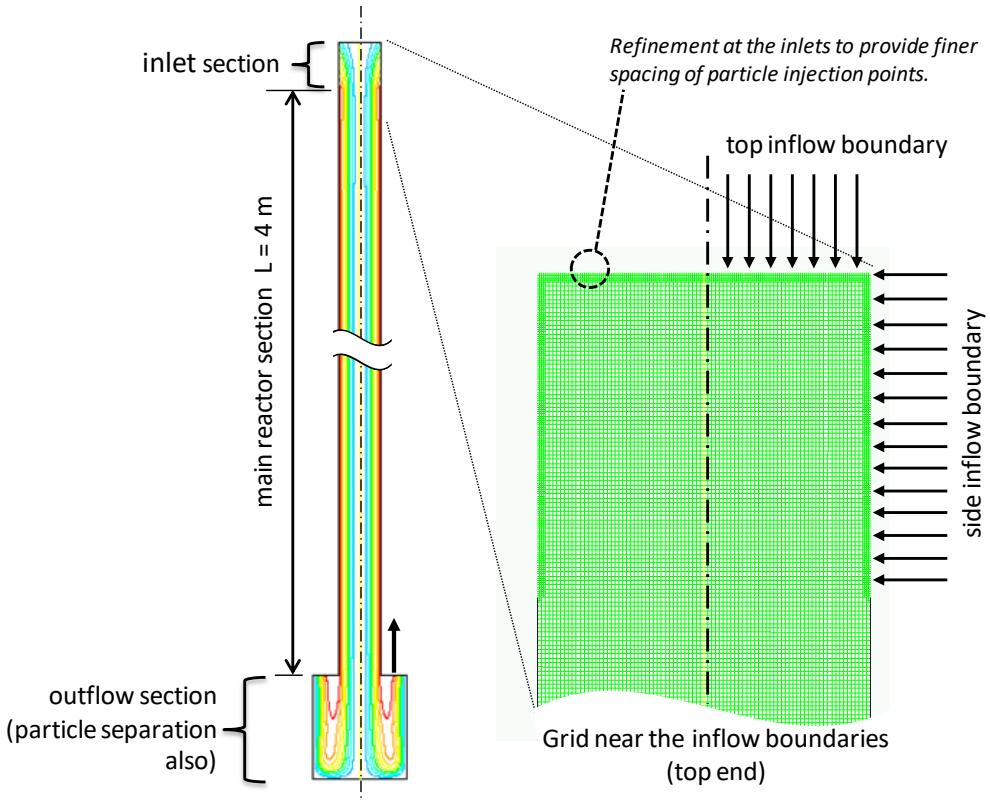

Figure 22. CFD model geometry for the carbonation reactor. A truncated depiction of the geometry is shown, for better use of space, while the symmetric half that is modelled is here mirrored across the symmetry axis for clarity. The outflow section is modelled as a rudimentary particle trap, with the fluid outflow being the upward-facing boundaries. The detail view of the inlet boundaries region (shown right) illustrates the boundary-adjacent grid refinement which serves to increase the number of tracer particles injected by the discrete phase algorithm.

A compressible ideal gas fluid model is chosen mainly in order to automatically account for the variable reactor operating pressure (and its variation as reactants are consumed) rather than for aerodynamic compressibility effects which can be completely neglected for the low speed flow expected.

6.2. Example results

The reactor geometry considered for initial CFD model studies is 160 mm diameter and 4 m length. The range of feed rates considered (12 – 50 kg hr^{-1} CaO) and the analogous feeds of CO_2 result in characteristic Reynolds numbers of ≈ 2000 and above. Given also the typical feed injection geometries involving nozzles significantly smaller than the reactor diameter, it is very likely that some turbulence will be generated and sustained in the flow, especially at the higher end of the range of feed rate.

The properties of the carrier fluid are taken to be those of pure CO_2. For the purposes of the initial CFD studies, it is assumed that 50% stoichiometric excess (relative to complete CaO carbonation) of CO_2 is injected with the CaO solids. Particle material properties are taken to be those of CaO.

Currently, the entire reactor pipe wall is considered as a single prescribed temperature boundary although two separate prescribed temperature zones (with a 100 mm transition length) have been implemented in the CFD model, as per the functional topology of the carbonator shown in Figure 22.

One of the salient features of the carbonator aerodynamics that was identified by the initial (i.e. without the chemical reaction incorporated) computations was the strong tendency for the entrained CaO solids to migrate to the reactor walls. This was found to be – in the computations – mainly due to turbophoresis since the inclusion of a swirl component to the inflow velocities (causing centrifugation) only slightly intensified this tendency. This tendency for the particles to concentrate near the periphery can be clearly discerned in the radial distributions of particle concentration at different stations along the downer reactor length, as shown in Figure 23. The initially central stream of particles (due to some peripheral inflow) begins to be re-distributed to the periphery as early as 0.5 m into the main reactor section.

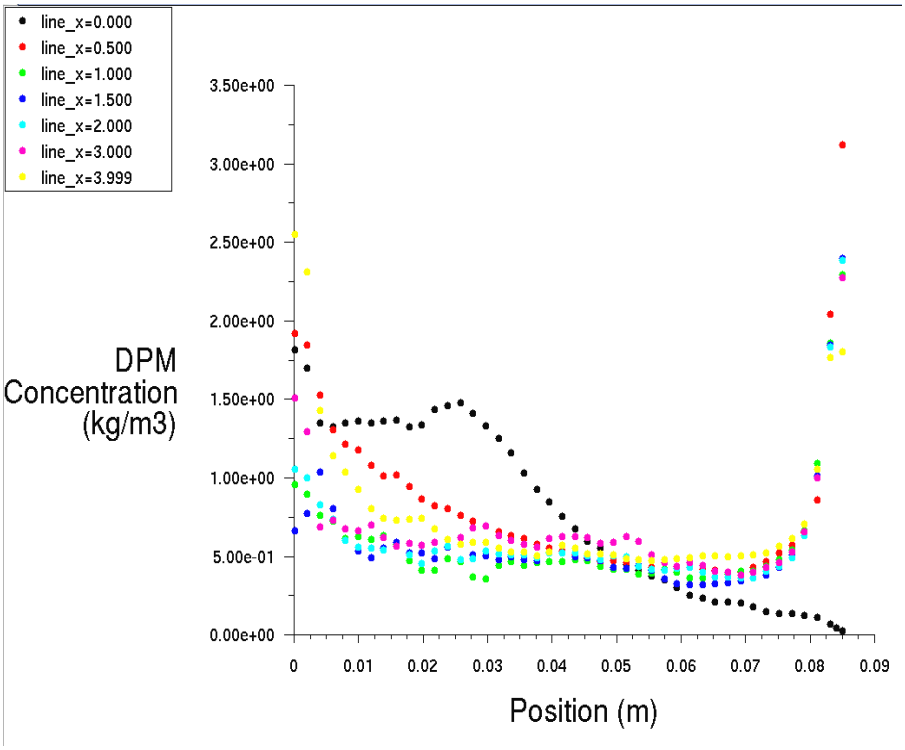

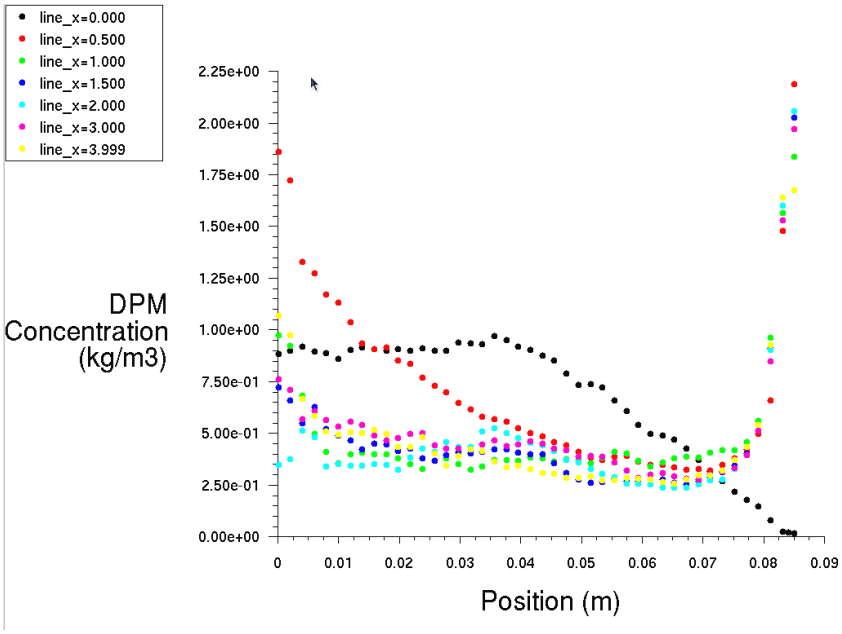

Figure 23. Solids ("Discrete Phase Model" or DPM) concentration vs. radial position at various stations along the reactor length (x-coordinate), for the case: CaO feed rate 25 kg hr^{-1}, CO_2 feed rate 29.4 kg hr^{-1}, inflow temperature 550 °C, wall temperature 350 °C. Results for both ø50 µm particles (top) and ø70 µm particles (bottom) are shown. The tendency for the particle to concentrate near the reactor wall (mainly due to turbophoresis) is evident in both cases.

Due to the two-way interaction of entrained solids and fluid flow, the peripheral concentration of the particles also gives rise to quite persistent flow pattern where there are regions of stagnant or even reverse flow in the reactor central region. A representative case can be seen in Figure 24. This flow pattern has been found to persist even in the case of a hot wall / colder inflow (200 °C difference) where the thermally induced buoyancy effects induce the opposite behaviour (peripheral reverse flow, central down-flow) in the absence of particles.

The flow patterns described pertain to the bulk of the entrained solids stream without excluding the presence of particles in all regions of the reactor, as can be seen in the particle traces seen in Figure 25 where only 5 particles per injection point are traced. It is evident that particles entrained near the center of the reactor inlet have a reduced affinity to the reactor periphery although – due to the turbulent dispersion – a fraction of particles from all injection positions will visit all reactor regions, i.e. no particle-free regions are predicted.

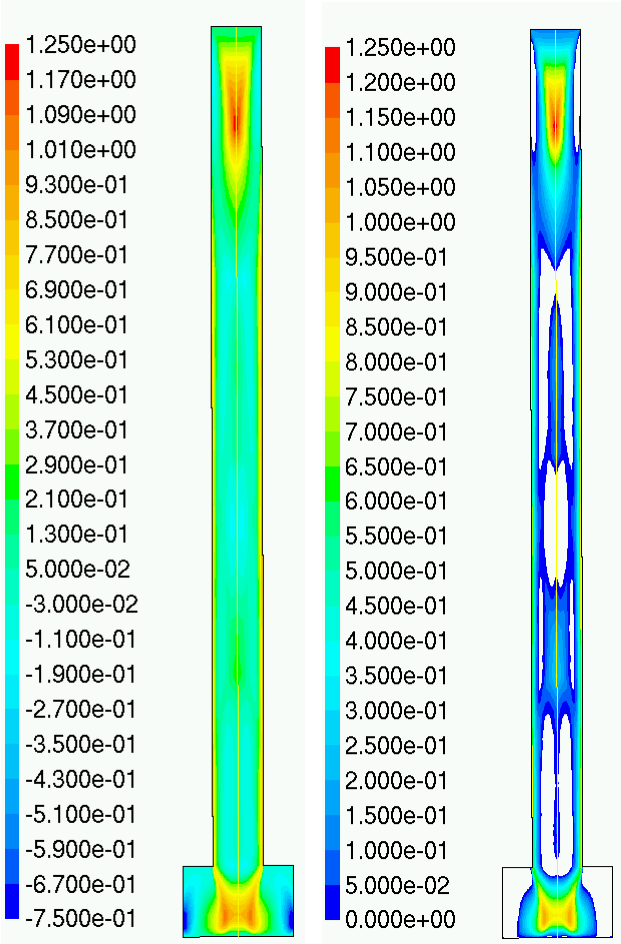

Figure 24. Contour plot of axial velocity for the case: CaO feed rate 25 kg hr^{-1} as ø70 µm particles, CO_2 feed rate 29.4 kg hr^{-1}, inflow temperature 550 °C, wall temperature 350 °C. The right plot illustrates the reverse flow regions by clipping the contours to the positive velocities only.

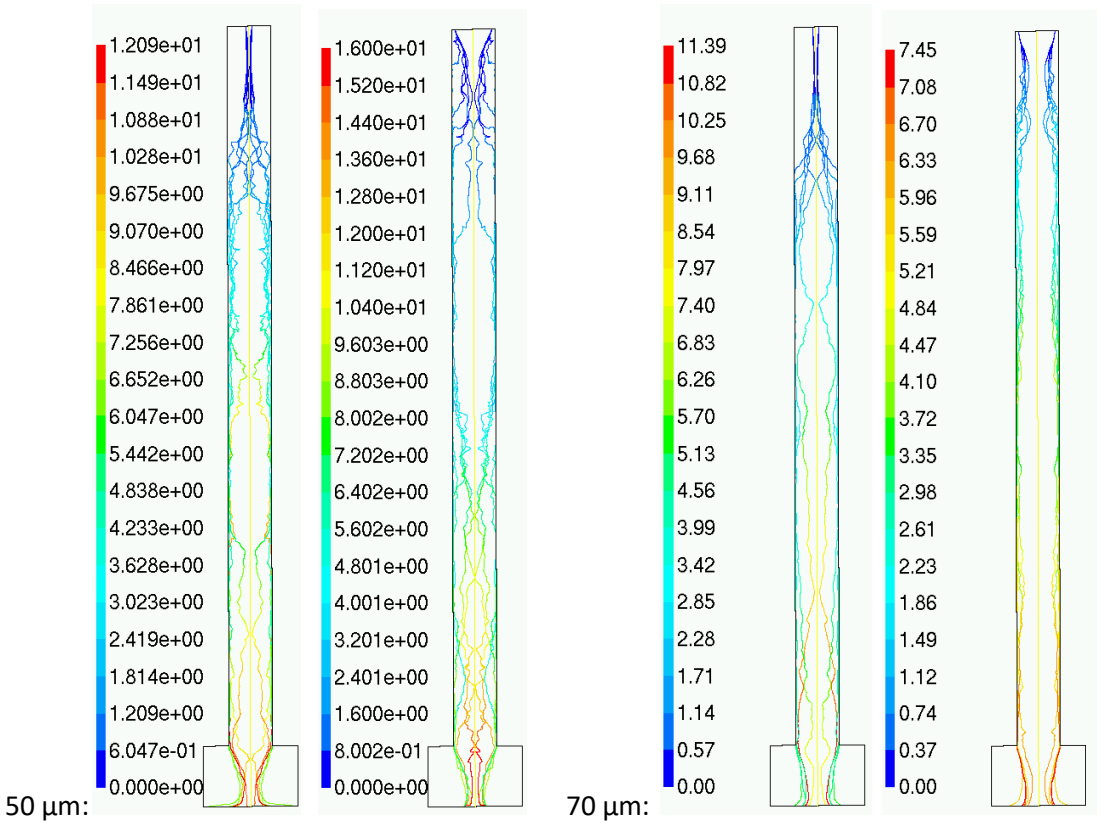

Figure 25. Selected illustrations of particle trajectories, for the case: CaO feed rate 25 kg hr^{-1}, CO_2 feed rate 29.4 kg hr^{-1}, inflow temperature 550 °C, wall temperature 350 °C. Results for both ø50 µm particles (left) and ø70 µm particles (right) are shown, for two different injections points (a central one and a peripheral one).

6.3. Working/optimal values of numerical parameters

The results of the CFD-based carbonator model depend on a rather extensive set of numerical parameters, due to the multiple physical (and chemical) phenomena which are involved and the numerous tow-way couplings between them. Trial computations within the nominal conditions (12.5 - 25 kg CaO hr^{-1}, 50% excess CO_2, inflow/wall temperatures 350 – 600 °C, operating pressure 1.7 bar) have been performed to determine the following optimal/working values of the relevant numerical parameters, shown in Table 18 below:

Table 19. Optimal model parameters within SOCRATCES nominal conditions.

Parameter description	**Criterion**	**Optimal values found**
Under-relaxation factor for the momentum equations	stability	0.6
Under-relaxation factor for turbulence variables	stability	0.6
Under-relaxation factor for body forces on the fluid	stability	0.7
Under-relaxation factor for pressure correction (continuity)	stability	0.7
Under-relaxation factor for the energy equation	stability	0.7
Particle injection point density on inflow boundaries	accuracy	1 mm
Number of stochastic trials per particle injection point	accuracy and stability	300

Under-relaxation factor for Discrete Particle Model source terms	stability	0.20
Particle tracking length scale	accuracy	3 mm
Maximum number of trajectory steps (per particle)	accuracy	14000

The above parameter values are expected to be suitable for the range of conditions relevant to the carbonation process considered in the SOCRATCES project. The accuracy-linked parameters invariably have a strong impact on computational overhead and so may be temporarily set to less strict values during preconditioning of newly initialised simulations in order to reduce calculation time.

7. REFERENCES

[1] R. Deng, H. Liu, F. Wei, and Y. Jin, "Axial flow structure at the varying superficial gas velocity in a downer reactor," *Chem. Eng. J.*, vol. 99, no. 1, pp. 5–14, 2004.

[2] Y. Cheng, C. Wu, J. Zhu, F. Wei, and Y. Jin, "Downer reactor: From fundamental study to industrial application," *Powder Technol.*, vol. 183, no. 3, pp. 364–384, 2008.

[3] B. Luo, D. Yan, Y. L. Ma, S. Barghi, and J. Zhu, "Characteristics of gas-solid mass transfer in a cocurrent downflow circulating fluidized bed reactor," *Chem. Eng. J.*, vol. 132, no. 1–3, pp. 9–15, 2007.

[4] Y. Bolkan, F. Berruti, J. Zhu, and B. Milne, "Modeling circulating fluidized bed downers," *Powder Technol.*, vol. 132, no. 2–3, pp. 85–100, 2003.

[5] J. S. Kasule, R. Turton, D. Bhattacharyya, and S. E. Zitney, "Mathematical modeling of a single-stage, downward-firing, entrained-flow gasifier," *Ind. Eng. Chem. Res.*, vol. 51, no. 18, pp. 6429–6440, 2012.

[6] M. Zeneli, A. Nikolopoulos, N. Nikolopoulos, P. Grammelis, S. Karellas, and E. Kakaras, "Simulation of the reacting flow within a pilot scale calciner by means of a three phase TFM model," *Fuel Process. Technol.*, vol. 162, pp. 105–125, 2017.

[7] Y. Cheng and C. H. Wang, "Numerical study on coal gasification in the downer reactor of a triple-bed combined circulating fluidized bed," *Ind. Eng. Chem. Res.*, vol. 53, no. 16, pp. 6624–6635, 2014.

[8] S. Vaishali, S. Roy, and P. L. Mills, "Hydrodynamic simulation of gas-solids downflow reactors," *Chem. Eng. Sci.*, vol. 63, no. 21, pp. 5107–5119, 2008.

[9] Y. Zhang, Y. Zhao, and X. He, "Modeling coal pyrolysis in a cocurrent downer reactor," *Particuology*, vol. 21, pp. 154–159, 2015.

[10] J. S. Kasule, R. Turton, D. Bhattacharyya, and S. E. Zitney, "One-dimensional dynamic modeling of a single-stage downward-firing entrained-flow coal gasifier," *Energy and Fuels*, vol. 28, no. 8, 2014.

[11] S. Wang, K. Luo, C. Hu, L. Sun, and J. Fan, "Impact of operating parameters on biomass gasification in a fluidized bed reactor: An Eulerian-Lagrangian approach," *Powder Technol.*, vol. 333, pp. 304–316, 2018.

[12] P. Khongprom, A. Aimdilokwong, S. Limtrakul, and T. Vatanatham, "Axial gas and solids mixing in a down flow circulating fluidized bed reactor based on CFD simulation," *Chem. Eng. Sci.*, vol. 73, pp. 8–19, 2012.

[13] A. Chuachuensuk, W. Paengjuntuek, S. Kheawhom, and A. Arpornwichanop, "A systematic model-based analysis of a downer regenerator in fluid catalytic cracking

processes," *Comput. Chem. Eng.*, vol. 49, pp. 136–145, 2013.

[14] Y. L. Yang, J. X. Zhu, Y. Jin, and Z. Q. Yu, "Investigation and modeling of cocurrent downflow circulating fluidized bed (downer)," *Chem. Eng. Commun.*, vol. 170, pp. 133–157, 1998.

[15] W. Liu, H. Li, and Q. Zhu, "Modeling the hydrodynamics of downer reactors based on the meso-scale structure," *Powder Technol.*, vol. 314, pp. 367–376, 2017.

[16] M. Spinelli, I. Martínez, and M. C. Romano, "One-dimensional model of entrained-flow carbonator for CO 2 capture in cement kilns by Calcium looping process," *Chem. Eng. Sci.*, vol. 191, pp. 100–114, 2018.

[17] M. Rhodes and Wiley InterScience (Online service), *Introduction to particle technology*. 2008.

[18] C. Wu, Y. Cheng, and Y. Jin, "Understanding riser and downer based fluid catalytic cracking processes by a comprehensive two-dimensional reactor model," *Ind. Eng. Chem. Res.*, vol. 48, no. 1, pp. 12–26, 2009.

[19] C. Ortiz, J. M. Valverde, R. Chacartegui, and L. A. Perez-Maqueda, "Carbonation of Limestone Derived CaO for Thermochemical Energy Storage: From Kinetics to Process Integration in Concentrating Solar Plants," *ACS Sustain. Chem. Eng.*, vol. 6, no. 5, pp. 6404–6417, 2018.

[20] M. A. Schöß, F. Schulenburg, and T. Turek, "reactions in a downer reactor – experiments and model-based analysis," *Chem. Eng. Sci.*, vol. 151, pp. 116–129, 2016.

[21] VDI, *VDI- Heat Atlas*. 2013.

[22] C. Ortiz, R. Chacartegui, J. M. Valverde, J. A. Becerra, and L. A. Perez-Maqueda, "A new model of the carbonator reactor in the calcium looping technology for post-combustion CO<inf>2</inf> capture," *Fuel*, vol. 160, pp. 328–338, 2015.

[23] B. Sarrion, J. M. Valverde, A. Perejon, L. Perez-Maqueda, and P. E. Sanchez-Jimenez, "On the Multicycle Activity of Natural Limestone/Dolomite for Thermochemical Energy Storage of Concentrated Solar Power," *Energy Technol.*, vol. 4, no. 8, pp. 1013–1019, 2016.

[24] J. C. Abanades and D. Alvarez, "Conversion limits in the reaction of CO2 with lime," *Energy and Fuels*, vol. 17, no. 2, pp. 308–315, 2003.

[25] E. Karasavvas, K. D. Panopoulos, S. Papadopoulou, and S. Voutetakis, "Design of an integrated CSP-calcium looping for uninterrupted power production through energy storage," *Chem. Eng. Trans.*, vol. 70, no. 2012, pp. 2131–2136, 2018.

[26] R. Chacartegui, A. Alovisio, C. Ortiz, J. M. Valverde, V. Verda, and J. A. Becerra, "Thermochemical energy storage of concentrated solar power by integration of the calcium looping process and a CO2 power cycle," *Appl. Energy*, vol. 173, pp. 589–605, 2016.

[27] A. Alovisio, R. Chacartegui, C. Ortiz, J. M. Valverde, and V. Verda, "Optimizing the CSP-Calcium Looping integration for Thermochemical Energy Storage," *Energy Convers. Manag.*, vol. 136, pp. 85–98, 2017.

[28] C. Y. Wen and T. Z. Chaung, "Entrainment Coal Gasification Modeling," *Ind. Eng. Chem. Process Des. Dev.*, vol. 18, no. 4, pp. 684–695, 1979.

[29] S. Kabelac and D. Vortmeyer, "VDI Heat Atlas Part K - Radiation," in *VDI Heat Atlas*, Second., VDI, Ed. Springer-Verlag Berlin Heidelberg, 2010.

[30] G. Nellis and S. Klein, *Heat transfer*. Cambridge University Press, 2008.

[31] ANSYS, "ANSYS Fluent Theory Guide v16," *ANSYS 16.2 Doc.*, vol. 15317, no. July, p. 80, 2015.

CONCLUSIONS

In this deliverable, a first stage carbonator model-based approach has been developed by CERTH and ZAR partners individually.

To begin with, CERTH partner developed a 1-D drop-tube carbonator model in steady-state conditions in order to perform simulations and evaluate carbonator performance under different operating and SOCRATCES conditions. The model simulates the solids and the gas as two separate phases, the gas and the solid phase, with individual physical properties each. Mass, energy and momentum equations are solved for both phases and are integrated with a kinetic model that has previously developed by AUTH (D2.1 and 1st WP2 internal report). Initial reactants temperature, pressure, mass flow rate of reactants, phases velocities and densities are some of the crucial inputs of the model. On the other hand, the most important outputs of the model constitute the sorbent and CO_2 conversion profile along the reactor, profile of carbonator temperature (gas and solid phase), variation of velocity (gas and solid phase) and energy transfer source terms. The latter refers to the energy produced due to exothermic carbonation reaction, the energy transferred from solids (where chemical energy produced and accumulated) to gas phase, and eventually the energy transferred from gas phase to the wall for the exploitation in the power block. As inferred from the model solution, carbonator performance is critically affected by operation variables such as initial reactants temperature, T_{in}, pressure P, reactor's wall temperature T_w, length and diameter of the reactor, L, D, CO_2 excess and maximum sorbent conversion Xk. The latter is stipulated by the number of calcination/carbonation cycles (i.e., 69.1% for the first cycle and 15% after the 10th cycle). Also, the same simulation activities were performed for two types of kinetics, the "slow" (1st WP2 internal report) and the "fast" one (D.2.1) assessing in this way the capabilities of the model under several operation condition and different kinetic regimes.

ZAR partner developed a 1-D PFR model for the gas phase and an entrained-flow model for the solid phase among with carbonation kinetics. Also, a mathematical model for the helical heat exchanger has being integrated predicting the temperature variation of the heat transfer fluid (CO_2). The results from the model described in this report (ZAR), when applied to the base case design, showed that the stoichiometric operation is not feasible. Moreover, it must be taken into account the great error introduced at time zero due to the kinetic model which gives an initial conversion of 5%. When only 10 kg h^{-1} of CO_2 are used as reactant, the carbonation reaction remains inhibited during most part of the carbonator length, and the reached temperatures are not proper for the material of which the reactor is made. Thus, the utilization of CO_2 excess is recommended in order to reduce the residence time and thus better distribute the exothermal heat of the reaction. Moreover, the excess CO_2 acts as a heat sink that helps cooling the reactor. However, it was found that the inlet temperature of the cooling fluids should be much greater than room temperature in order to achieve proper temperatures in the Stirling fluid and to obtain also more isothermal profiles in the carbonator. A proper configuration of CO_2 excess and inlet temperatures of the cooling fluids must be found to avoid the temperature limit of the carbonator's material and to reach the required temperature in the preheating of the CO_2 in the helical pipe of the upper carbonator. Moreover, the parametric analysis of the particle diameter shows that it has a negligible influence in the results. Lastly, for the case of using sintered CaO it is found that it would not be feasible to operate the base case design with this type of reactant. The results from the model described in this report (ZAR), when applied to the proposal of reducing the carbonator diameter, show that operation and cooling are feasible, leading to final conversions of 48%. Moreover, the temperature reached in the Stirling fluid is

enough for power production. However, it is found that carbonation reaction is inhibited at the end of the second carbonator. Regarding the parametric analyses presented, the avoidance of the carbonation inhibition is the most important aspect of the process. Increasing the mass flow of CO_2 in the helical pipe of the second carbonator allows reducing the inhibition of the reaction and thus increasing final conversions up to 64.4%. When sintered CaO is studied, the temperature profiles of both carbonators are kept in the range 800 – 865 °C, thus avoiding inhibition. However, the required specifications in the inlet temperatures of the cooling fluids to not reduce excessively the temperature in the carbonator may not be convenient in the prototype system.

Finally, CERTH developed a 2-D / axisymmetric CFD-based model which, in currently on-going work, will incorporate carbonation kinetics strongly coupled to the flow, heat and solids stream dynamics. In this way, a third carbonator model will become available, based on multi-physics CFD methods with, the prospect to verify a number of assumptions of the other two models (i.e., plug flow) and to give insights for better prediction of heat transfer coefficients. Also, the enhanced spatial detail of the CFD-based studies will comprise an additional valuable tool for the improved prototype carbonator design and construction. The next steps for the CFD-based model will include:

- Incorporation of the chemical kinetics model developed and validated within the project in order to account for the chemical reaction in the CFD and particle tracking simulation.
- Simulation with suitably simplified boundary conditions in order to be able to directly compare CFD-based carbonation results with those of lower dimensionality models developed in the project.
- Consideration of detailed aspects of the chemical reaction such as compositional and size variation of the particles due to spatial non-uniformities captured by the CFD-based model.
- Parametric studies with respect to CaO feedstock powder size distribution, reactor feed initial conditions as well as reactor thermal conditions (zone temperatures or heat abduction rate, etc.) to augment the results, from the simpler / one-dimensional reactor models, pertaining to particle temperature history, CaO conversion or other performance metrics.